REAL-TIME TSUNAMI INUNDATION FORECAST STUDY IN CHIMBOTE CITY, PERU

A Master's Thesis
Submitted in Partial Fulfillment of the Requirement
for the Master's Degree in Disaster Management

By
Nabilt Jill MOGGIANO ABURTO
(MEE16720)

August 2017

Disaster Management Policy Program
Seismology, Earthquake Engineering and Disaster-Recovery Management Policy & Tsunami Disaster Mitigation Courses (2016-2017)
Tsunami Disaster Mitigation Course

National Graduate Institute for Policy Studies (GRIPS),
Tokyo, Japan

International Institute of Seismology and Earthquake Engineering (IISEE),
Building Research Institute (BRI),
Tsukuba, Japan

ACKNOWLEDGEMENTS

I would like to express my sincere gratitude to my supervisor Prof. Kenji Satake and Dr. Aditya Gusman for supervising me and giving me very useful advice, guidance and suggestions during my individual study in the Earthquake Research Institute (ERI), The University of Tokyo. Besides my supervisor, I would like to express my sincere gratitude to my advisor Dr. Y. Fujii (IISEE/BRI) for his support and lectures at BRI. Thanks to all staff members at IISEE/BRI for their kind support and encouragement during this training program. Special thanks to my friends and colleagues from the Directorate of Hydrography and Navigation (DHN) and Universidad Nacional Mayor de San Marcos: Eng. Erick Ortega, Eng. Carol Estrada, Geo. Moises Molina, and Mg. Cesar Jimenez for your kind support and suggestions during elaboration of the thesis. To my friend Eng. Raquel Rios for trust on me and help me in remote sensing. Thanks to PhD. Juan Carlos Villegas-Lanza from Geophysical Institute of Peru for his comments of this manuscript. My gratitude to JAMSTEC staff for the guidance during the visit in Yokohama Institute of Earth Sciences-Japan Agency for Marine-Earth Science and Technology where the JAGURS code has been implemented. I would like to thanks to my friends Babita Sharma, Tara Pokarel and Letigia Corbafo for your company and enjoyable moments in Japan during this training. I would like to express my gratitude to JICA for giving me the opportunity to follow this master by financial supporting.

Finally, I would like to express my deepest gratitude and dedication of this research to my mother Luisa Aburto and my brother Charly Francia for their continued love, encouragement and support put on me from more than 15 000 km far away of my country (Peru). The guidance of my grandmother and grandfather are always with me.

ABSTRACT

For rapid forecast of tsunami inundation during a tsunamigenic event, we constructed pre-computed tsunami inundation database for Chimbote, which is one of the most populated cities in the north-central Peru and considered as a tsunami-prone area. The database consists of tsunami waveforms and modelled tsunami inundation areas based on a total of 165 fault model scenarios starting from 8.0 to 9.0 with an increment of 0.1 on moment magnitude scale (Mw). Following the methodology by Gusman et al. (2014) we evaluated the reliability of NearTIF algorithm using two hypothetical thrust earthquake scenarios: Mw 9.0 (worst-case event), Mw 8.5 (high probability of occurrence), and a finite fault model of the 1996 tsunami earthquake (Mw 7.6) offshore Chimbote. The linear tsunami propagation and nonlinear inundation were simulated with the JAGURS code implemented in a high-performance computer at Earthquake Information Center, Earthquake Research Institute, The University of Tokyo. This study demonstrated that NearTIF algorithm worked well even for tsunami earthquake scenario because it used a time shifting procedure for the best-fit fault model scenario searching. Finally, we evaluated the lead time with NearTIF algorithm for purpose of tsunami warning in Chimbote. Comparison of computation time indicated that NearTIF only needed less than 20 seconds while direct numerical forward modeling required 27-45 minutes. We thus demonstrated that NearTIF was a suitable algorithm for developing a future tsunami inundation forecasting system in Chimbote and would give useful contribution to improve and strengthen the Peruvian Tsunami Warning Center in terms of obtaining in short time a forecast of tsunami inundation maps for analysis of evacuation and reduction of loss of life.

Keywords: Real-time tsunami inundation forecast, Chimbote Peru

---

The author works for the Peruvian Tsunami Warning Center (CNAT, in Spanish), Directorate of Hydrography and Navigation (DHN), Callao, Peru

TABLE OF CONTENTS

LIST OF FIGURES

LIST OF TABLES

LIST OF ABBREVIATIONS

CNAT	Peruvian Tsunami Warning Center
DHN	Directorate of Hydrography and Navigation
EIC	Earthquake Information Center
ERI	Earthquake Research Institute
GEBCO	General Bathymetric Chart of the Oceans
IGP	Geophysical Institute of Peru
INDECI	National Civil Defense
INEI	National Institute of Statistics and Informatics
JAMSTEC	Japan Agency for Marine-Earth Science and Technology
MTH	Maximum Tsunami Height
NearTIF	Near-field Tsunami Inundation Forecasting
PLANAGERD	National Plan of Disaster Management Risk
PO-SNAT	Standard Operatives Procedures of the Peruvian Tsunami Warning System
SINAGERD	National System of Disaster Risk Management
SNAT	Peruvian Tsunami Warning System
SRTM3	Shuttle Radar Topography Mission
TTT	Tsunami Travel Time

1. INTRODUCTION

1.1. Background

The Republic of Peru, due to its geographic location on the western rim of South America, is permanently and highly exposed to natural phenomena such as landslides, avalanches, flooding, El Niño events, earthquakes, tsunamis and so on. Historical evidence confirmed that a number of tsunamis have struck the coast of Peru for the last 421 years, i.e.,1586, 1604, 1687, 1746, 1868, 1966, 1974 and recent events in 1996, 2001 and 2007. These events are the result of seismic activities associated with the Peru-Chile Trench, located approximately 160 km off the Peruvian coast, where the Nazca Plate is being subducted beneath the South American Plate. However, the instrumental and historical seismic catalog is insufficient for risk assessment, especially in the northern Peru. To conform with Hyogo Framework Action 2005-2015 and Sendai Framework for Disaster Risk Reduction 2015-2030, the National System of Disaster Risk Management (SINAGERD, in Spanish) in Peru under Law No. 29664 recommends working together for the objective to reduce the risk and protect lives and properties for sustainable development. In terms of tsunami, according to the National Plan of Disaster Management Risk 2014-2021(PLANAGERD, in Spanish), the people who live along the coast will be directly exposed to this natural hazard due to concentration of population, infrastructure and port activities. In this sense, in order to establish roles and responsibilities for each institution against the occurrence of earthquakes and tsunamis, the Standard Operatives Procedures of the Peruvian Tsunami Warning System (PO-SNAT, in Spanish) were signed on June, 2012 by three governmental institutions to conform with the Peruvian Tsunami Warning System (SNAT, in Spanish): The Geophysical Institute of Peru (IGP) in charge of monitoring the seismicity; the Directorate of Hydrography and Navigation (DHN) in charge of monitoring the sea level and issue tsunami bulletins (information, alert, alarm and/or cancellation); and the National Institute of Civil Defense (INDECI) in charge of distributing the tsunami warning information to citizens along the coast and to give assistance immediately in case of natural disasters. Through Supreme Decree No. 014-2011-RE, the DHN was appointed as the official representative of Peru to the International Tsunami Information Center with headquarters in Honolulu, Hawaii.

The Peruvian Tsunami Warning Center (CNAT, in Spanish) belongs to the DHN, whose headquarters is located in the Constitutional Province of Callao, Peru. The main activities of the CNAT are involved in tsunami warning as an important component of SNAT, besides making and updating tsunami inundation maps along the coast. In terms of tsunami risk, the main problem in the coastal area of Peru is the exposure to near-field tsunami, whose expected travel time is between 15 to 30 minutes.

According to PO-SNAT thresholds established in 2012, the CNAT have no more than 10 minutes to issue the tsunami bulletins. For the past few years, the first development of the software has made it possible to improve the time of issuing tsunami warning bulletins in short time (less than 3 min). The main software called "Pre-Tsunami" and developed by Jimenez (2010) forecasts the tsunami travel time (TTT) and maximum tsunami height (MTH) for tsunami warning. Since real-time forecast of tsunami inundation has not been implemented in Peru (even by any Tsunami Warning Center in South America), we need to improve a pre-computed tsunami inundation database by applying Near-Field Tsunami Inundation Forecasting (NearTIF) algorithm developed by Gusman et al. (2014) for this study in Chimbote city, Ancash Department, Peru.

1.2. Seismotectonic Settting

The seismotectonic setting of Peru is divided into three major segments (Silgado, 1978; Dorbath et al., 1990; Nishenko, 1991; Tavera and Buforn, 1998; Bilek, 2010, Villegas-Lanza et al., 2016): The first segment is the northern Peru, bounded by the Gulf of Guayaquil (from latitude 3°S to latitude 10°S); the second segment is the central Peru, which extends from the Mendaña fracture zone to the Nazca Ridge (10°S to ~15°S); and the third segment is the southern Peru, extending from the Nazca Ridge to the Arica bend (15°S to ~18°S) adjacent to the northern Chile segment, respectively.

The updated catalog of the large megathrust earthquakes in Peru by Villegas-Lanza et al. (2016) is shown in Figure 1, which means the absence of historical great earthquakes in the northern Peru segment and the sparse occurrence of moderate to large magnitude earthquakes might trigger local tsunamis along the Peruvian coast. The events occurred in 1619 (Mw ~7.7), 1953 (Mw 7.8), 1959 (Mw 7.5), 1960 (Mw 7.6), and 1996 (Mw 7.5) shown in Figure 1a were categorized as the largest subduction earthquakes reported so far in this region. Two of them had characteristics of tsunami earthquakes: a slow rupture velocity, long source time duration, and local tsunamis significantly greater than expected ones for their initial Ms values (Pelayo and Wiens, 1990; Ihmle et al., 1998; Bourgeois et al., 1999). Recently, the results with GPS campaign (2008-2013) by Villegas-Lanza et al. (2016) characterized the northern Peru to be shallow and weak to moderate coupling. These asperities have a good spatial correlation with the location of shallow rupture (Mw ~7.5) tsunami earthquakes that occurred in 1953, 1960, and 1996 respectively.

On the other hand, one of the lessons learned from the Great East Japan Earthquake and Tsunami Disaster caused by the Tohoku-Oki earthquake (Mw 9.0) of March 2011, is that the uncertainties in the shallow interseismic coupling should be taken into account in the following campaign. According to Villegas-Lanza et al. (2016), the moment deficit rate for the northern Peru segment (between Chiclayo and Chimbote) could vary significantly (from 0.1 to 0.4 x 10^{20} Nm/yr, ~Mw

6.6 - 7.0). Taking these uncertainties into account, we can infer that the cumulative moment deficit will reach the equivalent of Mw ~8.6 - 9.0 events in about 1000 years, while the occurrence interval is considered to be 500 years at the area where the 2011 Tohoku-Oki earthquake occurred (Sawai et al., 2015). Therefore, the authors conclude that, the seismic hazard in northern Peru should not be underestimated until seafloor GPS data are acquired and the shallow interseismic coupling is better evaluated for future research.

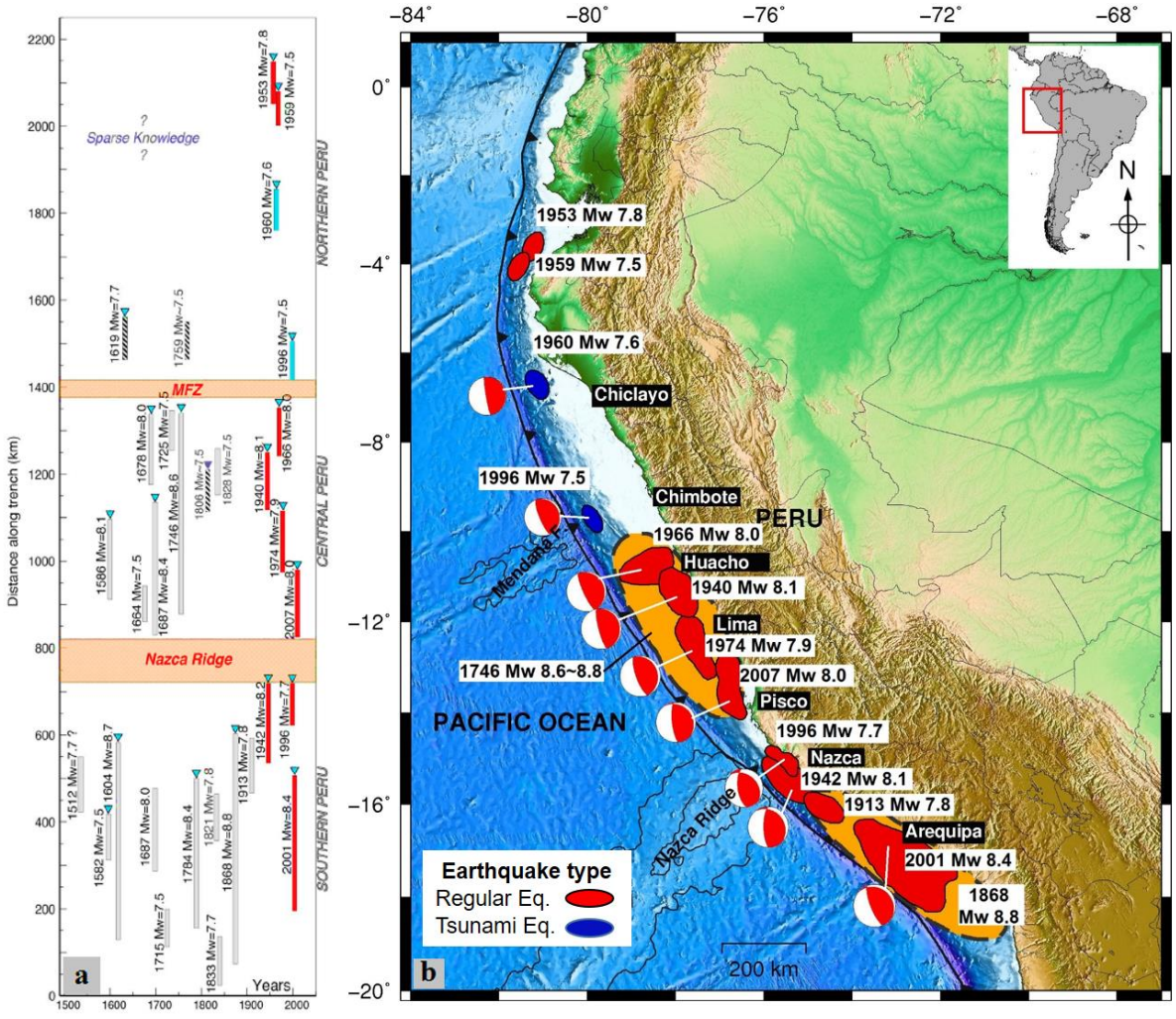

Figure 1. Historical seismicity in Peru. (a) Temporal and spatial distributions of large subduction earthquakes with Mw ≥ 7.5 that occurred in Peru since the sixteenth century, after Villegas-Lanza et al. (2016). (b) Seismotectonic setting for Peru subduction zone redrawn from Villegas-Lanza et al. (2016). The red ellipses indicate the approximate rupture areas of large subduction earthquakes (M ≥ 7.5) between 1868 and 2015. The blue ellipses indicate the locations of moderate tsunami earthquakes.

1.3. Characteristics of study area

Chimbote city is the capital of Santa Province, Department of Ancash. The city is located on the northeast coast of Chimbote Bay, south of Trujillo and at 420 km north of Lima in the North Pan-American highway. Chimbote has the largest fishing port in Peru, it is also known an important center in the country's fishing industry (more than 30 fish factories), port activities and a commercial center in the north-central Peru. Chimbote has the biggest population in the north-central Peru (193,154 residents according to INEI census, 2015) and is the third largest city along the Peruvian coast with an area of 26,565 km². Natural disasters occurred nearby Chimbote: the earthquake in 1970 (Mw 7.9), El Niño disaster in 1983 and the Chimbote tsunami earthquake (Mw 7.5) at 07:51 local time on February 21, 1996, about 130 km off the coast of northern Peru near the Peru–Chile Trench. This tsunami was caused by a slow rupture, a typical ''tsunami earthquake'' (Kanamori, 1972), and it led for the first time in Peru's history to an extensive post-tsunami field survey (Bourgeois et al., 1999), which indicated runup of ~5 m and damage to many houses/beach huts at Chimbote and 12 people in total were killed and injured by the tsunami (Heinrich et al., 1998).

The Chimbote Bay, also known as El Ferrol Bay, is a semi enclosed bay, surrounded by four islands: Blanca, Ferrol Norte, Ferrol Centro and Ferrol Sur; it has approximately 73.0 km^2, the greatest depths are identified at the surroundings of the main mouth; isobaths of 8 to 15 m predominate in the center. The Chimbote Bay is approximately 11.1 km long and 6.5 km wide.

1.4. Previous studies

This study follows recent publications "A methodology for near-field tsunami inundation forecasting: application to the 2011 Tohoku tsunami" by Gusman et al. (2014) and "Pre-computed tsunami inundation database and forecast simulation in Pelabuhan Ratu, Indonesia" by Setinoyo et al. (2017). The authors explain the concept of NearTIF as a methodology based on a pre-computed database of several tsunami waveforms at virtual points located off shore, and also tsunami inundation maps (with high-resolution topography and bathymetry) obtained by tsunami simulations of several fault model scenarios. In both publications, the authors explain that the most remarkable advantage of NearTIF is the rapid estimation (in a couple of minutes) to obtain tsunami inundation forecast in comparison with the direct numerical forward modeling. This means that this methodology is reliable and useful for tsunami warning purposes.

1.5. Purpose of this study

The main goal is to perform tsunami simulation with the NearTIF algorithm in order to achieve a real-time tsunami inundation forecast for Chimbote. We focus on Chimbote because it has the biggest population in the north-central Peru and economically, the main activities like fishing and port activities would be the most affected in case of tsunami. Chimbote is within the seismic gap characterized by the sparse knowledge of historical earthquakes triggering local tsunamis. Since no previous studies related to tsunami inundation forecast in this area, the Peruvian Tsunami Warning Center need to improve the time of response for tsunami evacuation in Chimbote.

The forecast of tsunami inundation maps in real-time based on pre-computed tsunami inundation database is carried out with the numerical simulation using accurate topography and bathymetry data, two hypothetical events (Mw 8.5 and Mw 9.0) and one tsunami earthquake scenario (Mw 7.6) by using the NearTIF algorithm for searching the best scenario and compare results with the forecasted ones.

2. DATA

2.1. Bathymetry Data

In order to perform simulation of tsunami propagation, bathymetry (submarine topography) data are needed. The global bathymetry was obtained from General Bathymetric Chart of the Oceans (GEBCO 2014) (Weatherall et al., 2015) with resolution of 30 arc-second. The finest grid to perform tsunami inundation is from bathymetry survey taken in 2015 and the Nautical Chart HIDRONAV No. 2123 by the Directorate of Hydrography and Navigation (DHN) map scale of 1:20,000 taken in 2009.

2.2. Topography Data

For the tsunami inundation on land, topography data are needed. Local topography data for tsunami inundation was derived from a topography survey done in 2015 by DHN with resolution of 10 m. To cover some part of the computational domain outside the surveyed area with topography data, we use the Shuttle Radar Topography Mission (SRTM3) data with resolution of 3 arc-second. Figure 2a shows topography and bathymetry data and Figure 2b shows the digital elevation model for Chimbote from raw data resampled into 1 arc-second of resolution used as finest domain (D4) in this research.

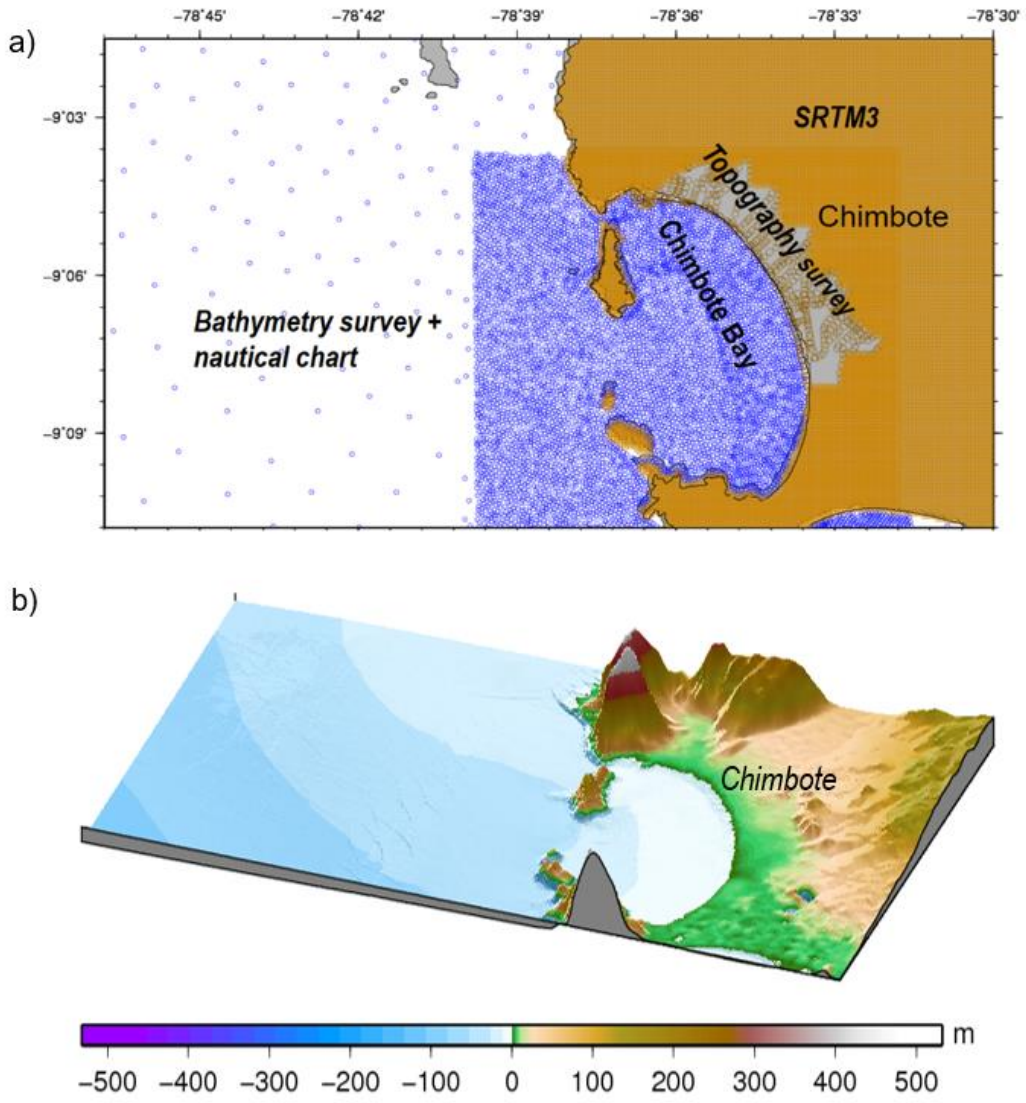

Figure 2. Data employed for tsunami simulation (a) Points of raw topography and bathymetry. (b) Digital elevation model for Chimbote used to compute tsunami inundation modeling.

3. METHODOLOGY

3.1. Introduction to NearTIF algorithm

Near-Field **T**sunami **I**nundation **F**orecasting, hereafter "NearTIF" is an algorithm and a methodology developed by Gusman et al. (2014) based on the assumption that if different earthquakes produce the similar tsunami waveforms at nearshore sites, then tsunami inundations in coastal areas will have similar

characteristics independent of their arrival time, location or source mechanism (Setinoyo et al., 2017). Three main components constitute the NearTIF algorithm: (1) the pre-computed tsunami database for tsunami waveforms and tsunami inundation, (2) the tsunami numerical model that solves the linear shallow water equations, and (3) the tsunami database search engine. Figure 3 shows the scheme of NearTIF method. In order to construct the tsunami database, we follow the procedures according to Gusman et al. (2014) in the next sections.

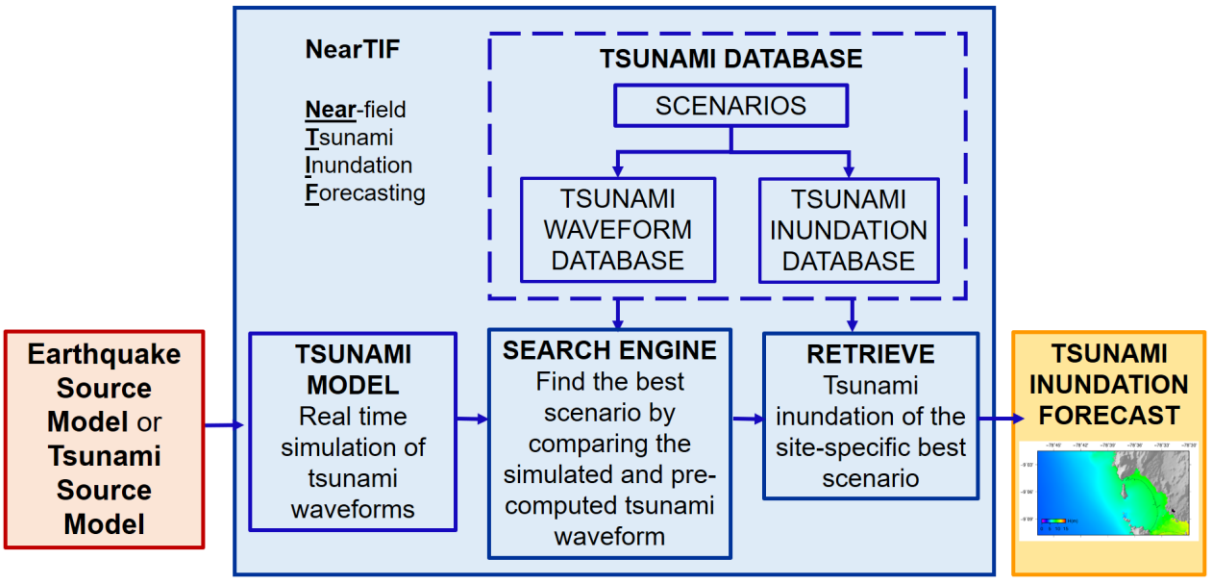

Figure 3. Scheme of NearTIF method, redrawn based on Gusman et al. (2014).

3.2. Fault Model Scenarios for Tsunami Database

To construct a tsunami database, we started by setting 15 reference points and specify the top and center of the fault plane, along the subduction zone off western Chimbote city (Figure 4). To construct the fault scenarios, we need the seismic parameters for each fault model, which means, length (L), width (W), top depth, strike, dip, rake, slip, latitude and longitude of top left corner (or center) of the fault plane. Basically, L and W were derived from Hanks and Bakun (2002) scaling relation, whose formula is Mw=4/3 log A + 3.03, where A is the fault area given by L=2 x W according to Gusman et al. (2014). Depth and dip angles were derived from interpolation of Slab Model for Subduction Zone (SLAB 1.0) of the South America region (Hayes et al., 2012), which was downloaded from the USGS web site (https://earthquake.usgs.gov/data/slab/). The slip amount was calculated from the seismic moment (Mo) using the formula of Mo=μAD (Kanamori, 1977; Hanks and Kanamori, 1979), where A is the area of the rupture in m^2, D is the displacement in m and μ is the rigidity along the plate interface, in this study we assumed 4 x 10^{10} Nm^{-2} for thrust earthquakes. We assumed a rake of 90° and the value for strike is

331°. The magnitude range used for each scenario started from Mw 8.0 to Mw 9.0 with increment of 0.1 magnitude unit, i.e., 11 scenarios with different sizes, following the methodology by Gusman et al. (2014). In total, 165 scenarios at 15 referents point with 11 different sizes were built. In Appendix-A Table A-1 shows the fault model parameters of each scenario.

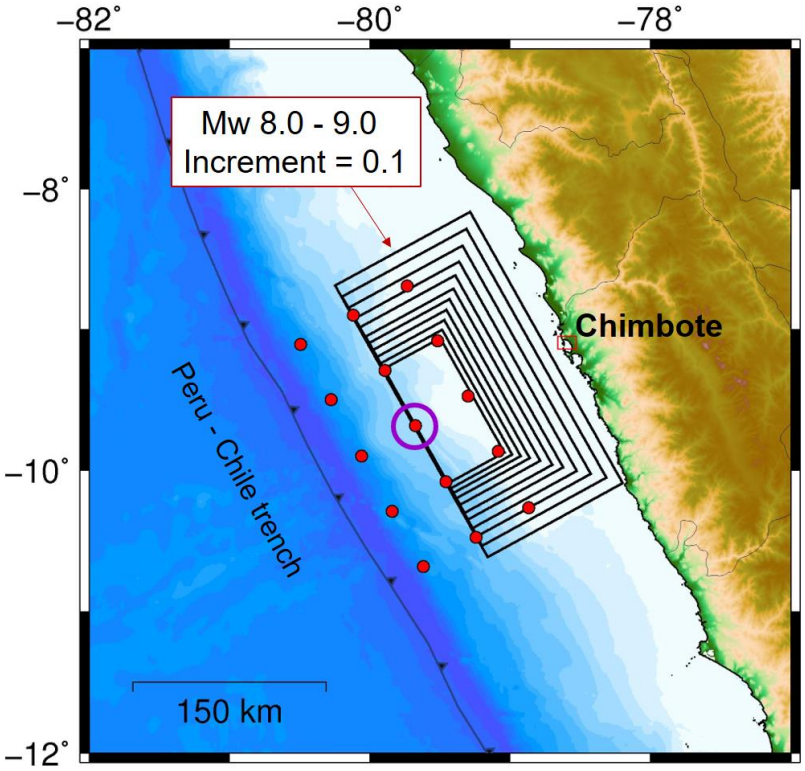

Figure 4. Fault models scenarios for constructing pre-computed tsunami waveform and tsunami inundation database. Red dots represent the 15 referent points. Black rectangles are examples of fault models with different fault sizes from Mw 8.0-9.0 A purple circle is on the top center of each fault model scenario.

3.3. Selection of Virtual Observation Points

A distribution of nine Virtual Observation Points (VOPs) was selected in front of Chimbote Bay (Figure 5) for the purpose of precompute tsunami waveform database using linear waves for tsunami propagation. The deepest VOP is No. 3 and its corresponding depth is 67 m (78.75° W, 9.127° S), and the shallowest VOP is No.7 at 25 m (78.674°W, 9.075° S). The distance between respective observation points is 50 km. According to Gusman et al. (2014), the importance of VOPs is to obtain information

on directivity of tsunami propagation, which is also related with tsunami inundation on land, at multiple observation points. These VOPs are all virtual points and no actual instrumentation is required.

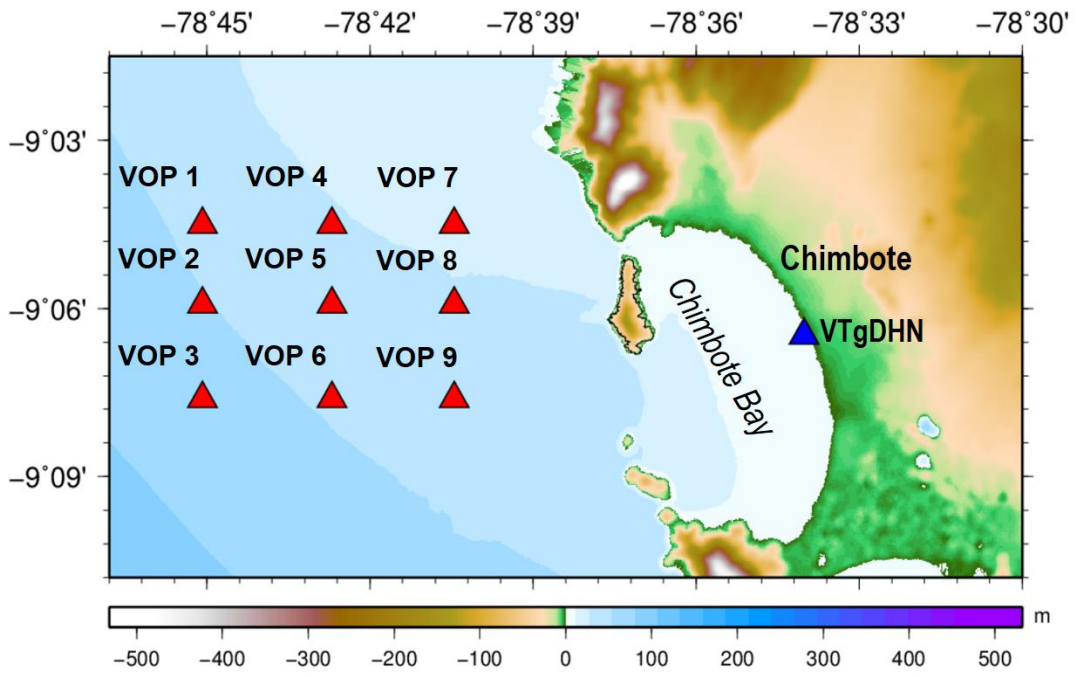

Figure 5. Distribution of nine VOPs (red triangles) off Chimbote Bay. The virtual tide gauge of DHN "VTgDHN" is not considered in the methodology of NearTIF because it is only for the purpose to obtain the tsunami arrival time near the coast of Chimbote.

3.4. Tsunami Numerical Simulation

In order to compute the offshore tsunami waveforms and tsunami inundation to be stored in the database we use JAGURS code to computes linear and nonlinear shallow water equations with a finite difference scheme in spherical coordinates. **JAGURS** was developed under a collaboration among **JA**MSTEC (Japan Agency for Marine-Earth Science and Technology) which was developed and parallelized by **G**eoscience Australia and **UR**S Corporation (United Research Services, California) using **S**atake's kernel (Baba et al., 2014). The code is written in Fortran 90 with parallelization by using message-passing interface (MPI) and opening multi-processing (OpenMP) libraries. The JAGURS code was implemented on high performance computer at Earthquake Information Center (EIC), Earthquake Research Institute (ERI), The University of Tokyo.

JAGURS is a numerical code that computes tsunami propagation and inundation on the basis of the long waves. These are solved on a finite difference scheme using a staggered grid and the

leapfrog method. The calculations can be performed in a spherical coordinate system or a Cartesian coordinate system and nesting of terrain grids (Baba and Cummins, 2016).

The governing equations explained in Baba et al. (2015a) are given by:

$$\frac{\partial M}{\partial t}+\frac{1}{Rsin\theta}\frac{\partial}{\partial \varphi}\left(\frac{M^2}{d+h}\right)+\frac{1}{R}\frac{\partial}{\partial \theta}\left(\frac{MN}{d+h}\right)=-\frac{g(d+h)}{Rsin\theta}\frac{\partial h}{\partial \varphi}-fN-\frac{gn^2}{(d+h)^{7/3}}M\sqrt{M^2+N^2}$$
$$+\frac{d^2}{3Rsin\theta}\frac{\partial}{\partial \varphi}\left[\frac{1}{Rsin\theta}\left(\frac{\partial^2 M}{\partial \varphi \partial t}+\frac{\partial^2 (Nsin\theta)}{\partial \theta \partial t}\right)\right] \quad (1)$$

$$\frac{\partial N}{\partial t}+\frac{1}{Rsin\theta}\frac{\partial}{\partial \varphi}\left(\frac{MN}{d+h}\right)+\frac{1}{R}\frac{\partial}{\partial \theta}\left(\frac{N^2}{d+h}\right)=-\frac{g(d+h)}{R}\frac{\partial h}{\partial \theta}+fM-\frac{gn^2}{(d+h)^{7/3}}N\sqrt{M^2+N^2}$$
$$+\frac{d^2}{3R}\frac{\partial}{\partial \theta}\left[\frac{1}{Rsin\theta}\left(\frac{\partial^2 M}{\partial \varphi \partial t}+\frac{\partial^2 (Nsin\theta)}{\partial \theta \partial t}\right)\right] \quad (2)$$

$$\frac{\partial h}{\partial t}=-\frac{1}{Rsin\theta}\left[\left(\frac{\partial M}{\partial \varphi}+\frac{\partial (Nsin\theta)}{\partial \theta}\right)\right] \quad (3)$$

$$M=(d+h)u \quad (4)$$

$$N=(d+h)v \quad (5)$$

The variables M and N are depth-integrated quantities equal to $(d+h)u$ and $(d+h)v$, respectively, along longitude and latitude lines; h is water height from the sea surface at rest, t is the time, θ and φ are co-latitude and longitude, g is the gravitational constant, R is the earth's radius, n is Manning's roughness coefficient, f is the Coriolis parameter (this parameter and dispersion term were not used in the present research).

3.4.1. Finite-difference scheme

According to Baba et al. (2015b), to compute tsunami propagation and areas of inundation using the JAGURS code, Equations (1) - (5) are solved by the finite-difference method using spherical coordinates. To solve these equations, we used the leapfrog, staggered-grid, finite-difference calculation scheme. Tsunami inundation on the land is modeled by a moving wet or dry boundary condition (Kotani et al., 1998). The computational time step is determined by the Courant–Friendrichs–Lewy condition (CFL) for a staggered-grid scheme: $dt < \Delta x/\sqrt{2gh_{max}}$, where g is the gravity, h_{max} is the maximum water depth and Δx is grid spacing of each computational domain. We used a constant time step dt = 0.4 for the entire calculation (6 h) which satisfied the CFL condition among those of the nested grids (Table 1).

The bottom friction between the fluid and the land is given by Manning's roughness coefficient (Table 2), in this study we adopted a uniform value of 0.0025 $m^{-1/3}$ s on the grid system (after Linsey and Franzini, 1979; Baba et al., 2014). The propagation time of 6 hours has been chosen in order to simulate a significant length of tsunami waveforms and maximum tsunami inundation to be stored in the database.

Table 1. Computational domains for JAGURS.

ID	Grid Δx (sec)	Grid Δx (m)	zmax (m)	CFL (s)	dt (s)
D1	27	833.96	6702.03	2.30	0.4
D2	9	277.98	6360.35	0.78	
D3	3	92.66	138.64	1.77	
D4	1	30.88	86.45	0.75	

Table 2. Values for Manning's roughness coefficient (n), after Linsley and Franzini (1979).

Channel Material	n ($m^{-1/3}$ s)
Neat cement, smooth metal	0.010
Rubble masonry	0.017
Smooth earth	0.018
Natural channels in good condition	0.025
Natural channels with stones and weeds	0.035
Very poor natural channels	0.060

3.4.2. Nesting Grids

Four domains (D1 to D4) form the nested grids system, were defined for our study area as shown in Figure 6. The coarsest grid represents the entire computational Domain No. 1 (D1) from 85.0°W to 76.0° W and from 14.5°S to 5.5°S, including the tsunami source and the target area of Chimbote city, Peru. Global bathymetry and topography were made with GEBCO 2014 Grid data, which was interpolated to 27 arc-sec intervals (~833 m, 1200 x 1200 grid nodes). These datasets were also subsampled and interpolated, respectively, to make grids for Domain No. 2 (D2) with spacing of 9 arc (~277 m, 805 x 721 grid nodes) and Domain No. 3 (D3) with 3 arc-sec for the nesting scheme (~92 m, 853 x 781 grid nodes). The finest grid for topography and bathymetry which correspond to Domain No. 4 (D4) including area around the Chimbote Bay was made using a combination of the DHN's multi-narrow beam surveys and nautical chart conducted in 2015; the topography grid was made with DHN's topography survey conducted in 2015 and SRTM3 (Shuttle Radar Topography Mission) by Jarvis et al. (2008) for areas where it was not possible to obtain data *in situ*; all this information was interpolated to 1 arc-sec intervals (~30 m, 1009 x 559 grid nodes). The nesting grids system were used to compute

tsunami propagation by solving the linear shallow water waves for domains D1 to D3 and tsunami inundation by solving the nonlinear shallow water waves in the finest domain (D4).

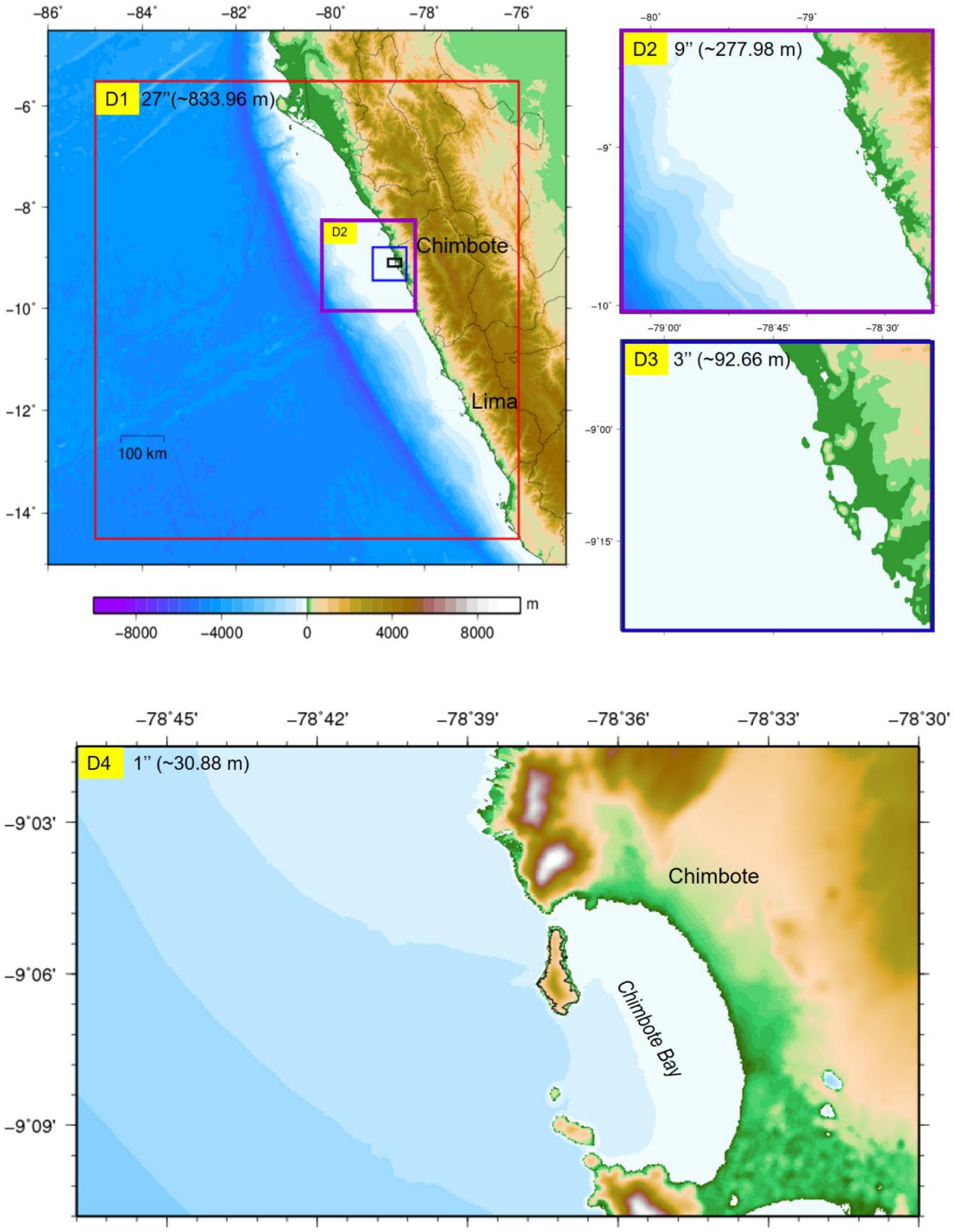

Figure 6. Nesting grids of four domains (D1, D2, D3 and D4) used for tsunami simulation using JAGURS. Domain D4 represents the finest grid for tsunami inundation database.

3.5. Construction of Tsunami Waveform and Tsunami Inundation Database

Tsunami waveforms and tsunami inundation are the most important components for the NearTIF tsunami database. Tsunami waveforms at nine VOPs off the coast of Chimbote Bay were computed by solving linear long waves equations with a finite-difference scheme for a coarse domain No. 1 (D1) of 1 arc-min (~1853 m) resolution. To construct the waveforms, 165 fault model scenarios (described in section 3.2) were used as input files. The output is a pre-computed tsunami waveform database (Figure 7) which is used in the NearTIF algorithm to search the best-fit fault model scenarios. On the other hand, the tsunami inundation database was computed by solving nonlinear shallow wave equations with a finite-difference scheme. We construct tsunami inundations with 165 fault model scenarios as input files; the finest domain (D4) of 1 arc-sec (~ 30 m) resolution corresponds to Chimbote city as a target area. The output is a pre-computed tsunami inundation database (Figure 8) which is used in the NearTIF algorithm to produce the tsunami inundation forecast map selected from the best specific fault model scenario. The JAGURS code in serial version was used for simulation of tsunami propagation (linear) and inundation (nonlinear).

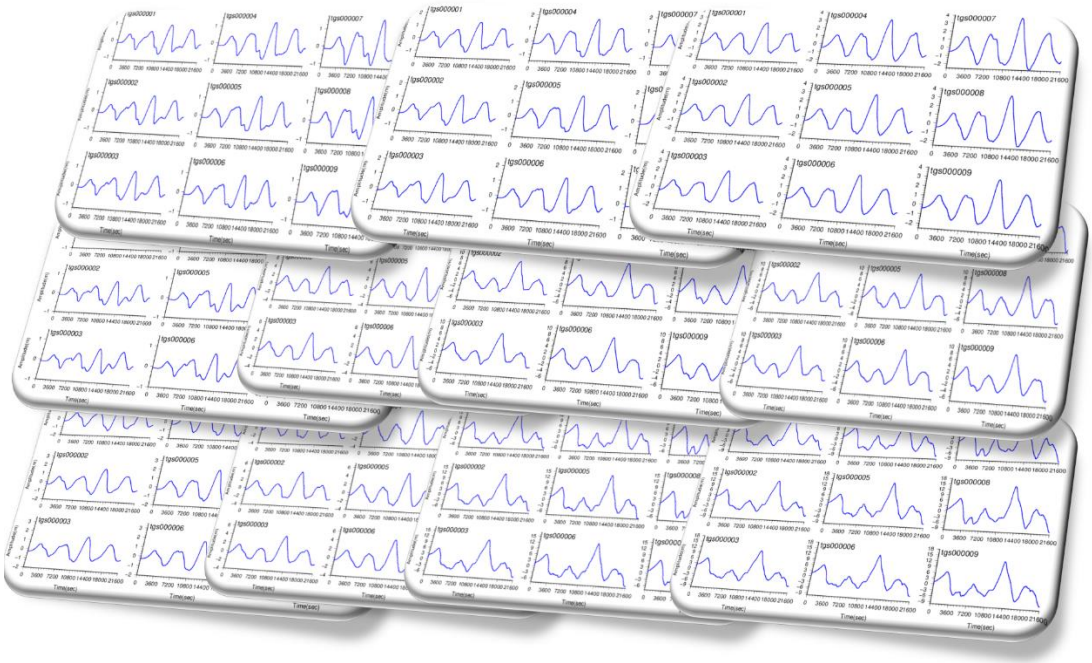

Figure 7. Illustration of the pre-computed tsunami waveforms to be stored in the tsunami waveform database (TWD).

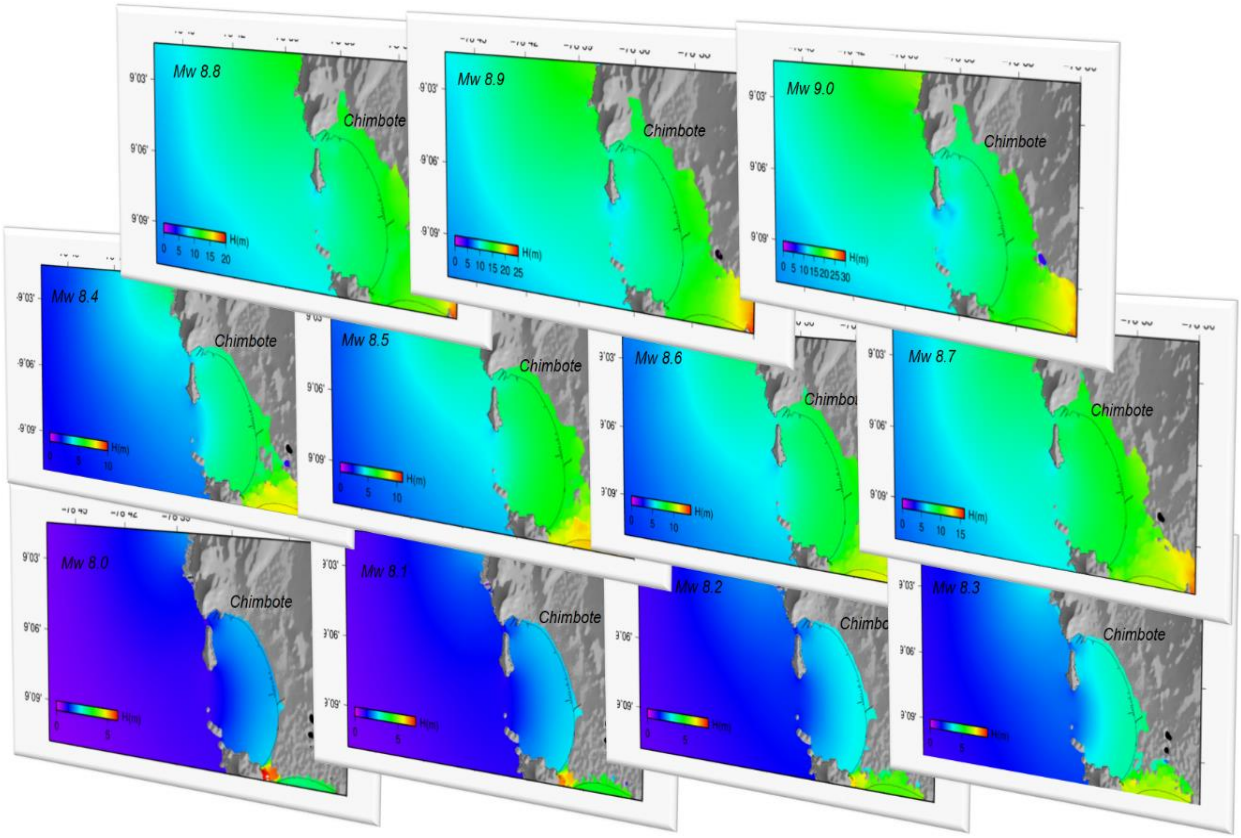

Figure 8. Illustration of the pre-computed tsunami inundation for tsunami inundation database (TID).

3.6. Hypothetical and Tsunami Earthquake Scenarios

To validate the NearTIF algorithm, we construct three earthquakes scenarios as input fault model, two of which are hypothetical thrust earthquakes, case 1: Mw 9.0 (worst-case scenario) and case 2: Mw 8.5 (high probability of occurrence). The third scenario (case 3) is a finite fault model of tsunami earthquake (Mw 7.6) for offshore Chimbote in 1996 composed of 28 sub-faults based on teleseismic waveform inversion (Jimenez et al., 2015). Figure 9 shows the hypothetical and fault model scenarios and Table 3 summarizes the fault parameters for these scenarios.

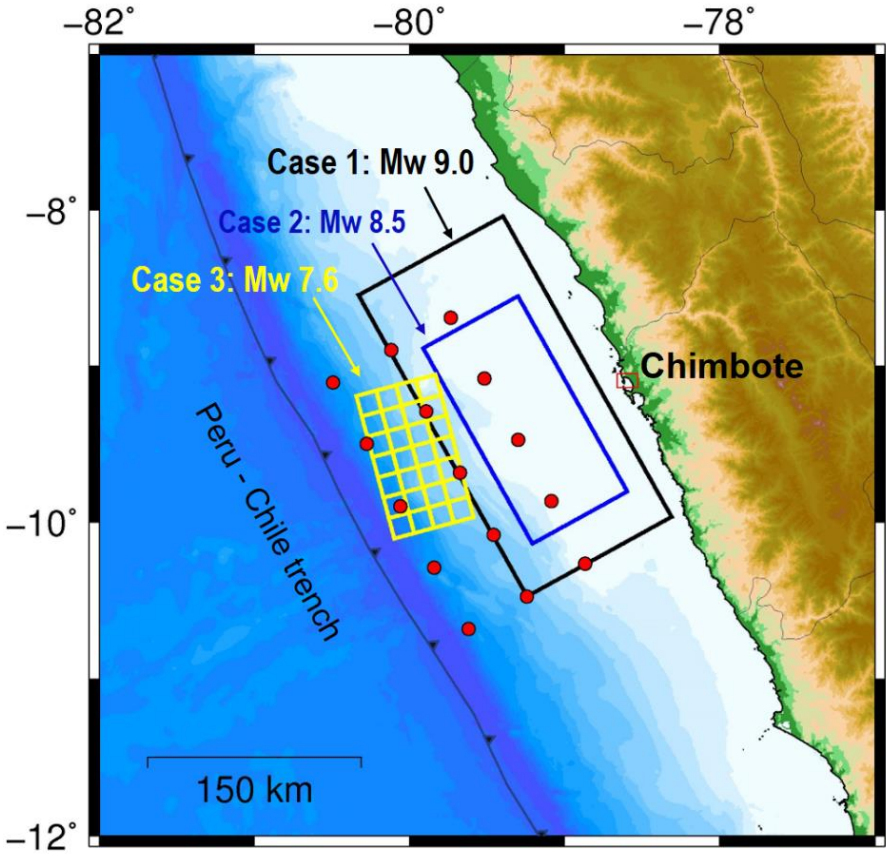

Figure 9. Location of hypothetical and tsunami earthquake scenarios. A black rectangle represents the worst scenario (Mw 9.0), a blue rectangle is considered as a probable scenario for Chimbote city (Mw 8.5) and yellow lines draw the finite fault model of 1996 Chimbote tsunami earthquake (Mw 7.6) by Jimenez et al. (2015).

Table 3. Fault parameters of hypothetical and tsunami earthquake scenarios.

Case	M_w	Fault Location		Length	Width	Strike	Dip	Rake	Slip	Top depth
		Lon (°W)	Lat (°S)	(km)	(km)	(deg)	(deg)	(deg)	(m)	(km)
1	9.0	-79.2417	-10.4750	245.1	122.5	331	18	90	33.1	8.0
2	8.5	-79.2069	-10.1386	159.1	79.6	331	18	90	14.0	10.0
3	7.6	Finite fault model (28 sub-faults) of Chimbote tsunami earthquake (Mw 7.6) in 1996 by Jimenez et al., (2015) shown in Table B-3, Appendix-B.								

The parameters of the fault models scenarios (Tables B-1, B-2, B-3 in Appendix-B) were used to calculate the initial sea surface elevation in an elastic half-space (Okada, 1985), which is the initial condition for numerical tsunami simulation. The effect of the horizontal displacement to the initial sea surface elevation (Tanioka and Satake 1996) is included.

3.7. Tsunami Database Search Engine

After an earthquake occurs (near-field scenarios in this study) and the seismic parameters of the fault model are available, tsunami waveforms at the virtual observation points can be simulated by solving the linear shallow water equations using a finite difference scheme on the 1 arc-min for a coarse domain (D1) in less than 20 seconds by a serial computation using JAGURS tsunami code on the EIC high-performance computer. The candidate for the site-specific best scenario among 165 scenarios should give the most similar tsunami waveforms to a real tsunami (or tsunami waveforms from hypothetical scenarios considered in this study). The comparison can be made by RMS (root-mean-square) misfit/error analysis. In order to speed up the process, the NearTIF algorithm analyzes only an ensemble of tsunami waveforms within a threshold of 30% from the reference with the mean of maximum heights. A time window based on two cycles of tsunami waveforms is used for the RMS analysis in which wave cycles are automatically detected by the zero up/down crossing method. These processes are included in the "Tsunami Database Search Engine (TDSE)".

NearTIF TDSE uses an optimal time shift (τ_o) to shift the tsunami waveforms in order to get the minimum RMS misfit and avoid bad misfits due to the wave phase differences during the direct comparison between the pre-computed tsunami waveforms in the database and the real tsunami waveforms (or computed ones from hypothetical earthquakes). In this sense, every scenario will have an RMSE for evaluation. Following this procedure explained in Gusman et al. (2014), the scenario which gives the smallest RMSE value is selected as the site-specific best scenario among the NearTIF database. Finally, the pre-computed tsunami inundation of the best site-specific fault model scenario is selected as the tsunami inundation forecast, in this study for Chimbote city.

4. RESULTS AND DISCUSSION

We analyze the performance and effectiveness of the NearTIF algorithm by comparing the tsunami inundation maps from the database with tsunami inundation maps obtained by direct Numerical Forward Modeling (NFM) for each hypothetical earthquake (Mw 9.0 and Mw 8.5, respectively) and a tsunami

earthquake scenario (Mw 7.6). We also evaluate the lead time with the NearTIF algorithm for purpose of tsunami early warning forecasting in Chimbote.

4.1. NearTIF Computational Comparison with Numerical Forward Modeling (NFM)

The NearTIF algorithm first computes tsunami waveforms at VOPs by linear long wave simulation. Simulation of six hours with linear long waves on the 1 arc-min grid system (Domain 1 in Figure 6) using JAGURS code in a serial version on the EIC high-performance computer requires no more than 19 seconds of computational time. The algorithm then searches the best-fit fault model scenario from the database which produces the most similar tsunami waveform obtained from linear long wave simulation. Searching the best scenario requires only a few seconds to finalize. The tsunami inundation map from the best-fit fault model scenario is selected as the tsunami inundation forecast. In this study, the total time required to obtain tsunami inundation forecast map using the NearTIF algorithm is less than 20 seconds as shown in Table 4.

Table 4. Computational time lead for tsunami simulation.

Seismic Event	Numerical Forward Modeling (NFM)	NearTIF			
		Tsunami Model (Lineal computation)	Search Engine	Total time	Speed of NearTIF relative to NFM
Mw 9.0	45 min	19 sec	0.8 sec	19.8 sec	135 times faster
Mw 8.5	40 min	18 sec	1.5 sec	19.5 sec	120 times faster
Mw 7.6	27 min	14 sec	0.8 sec	14.8 sec	108 times faster

4.2. Case 1: The Offshore Chimbote Hypothetical Megathrust Earthquake (Mw 9.0)

A simple fault model for the hypothetical megathrust earthquake (Mw 9.0) was used offshore Chimbote (21 km off the coast of Chimbote) as a near-field tsunami case (Figure 10). We calculate the tsunami waveforms at nine virtual observation points (VOPs) offshore Chimbote by solving linear shallow water equations. To find the best-fit fault model scenario, the NearTIF algorithm searches the most similar tsunami waveform with minimum root-mean-square (RMSE) in the entire database (Figure 11a and 11b). As a result, the fault model scenario (FMS) No. 77 (Mw 9.0) is selected as the best site-specific FMS. Finally, the tsunami inundation result from FMS No. 77 is extracted from the database as a tsunami inundation forecast map for Chimbote. Figure 12 shows comparison of the tsunami waveforms computed by simulation of linear shallow water waves at nine VOPs from the hypothetical earthquake

of Mw 9.0 and those from FMS No. 77. Figure 13a and 13b shows the comparison of inundation areas from the hypothetical event and fault model scenario No. 77, which are very similar. In Appendix-B, Table B-1 and Figure B-1 show the fault model parameters and vertical displacement of FMS No. 77 and hypothetical megathrust earthquake Mw 9.0.

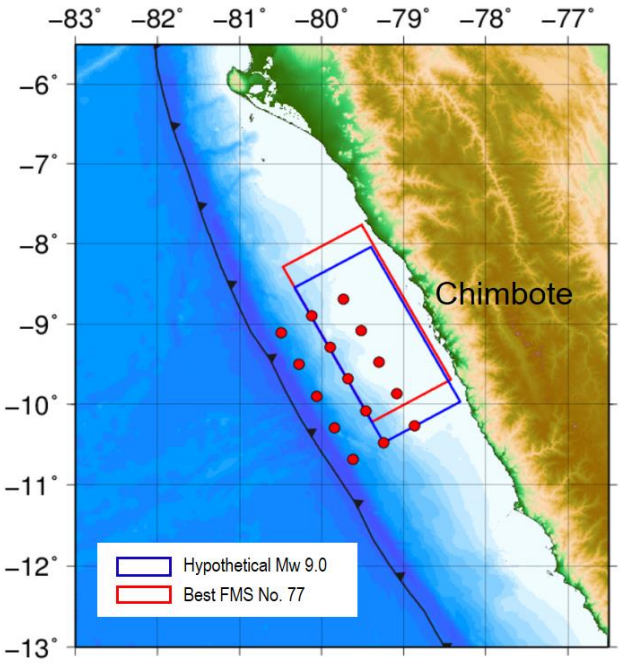

Figure 10. Location of hypothetical megathrust earthquake Mw 9.0 (blue rectangle) and the best FMS No. 77 (red rectangle).

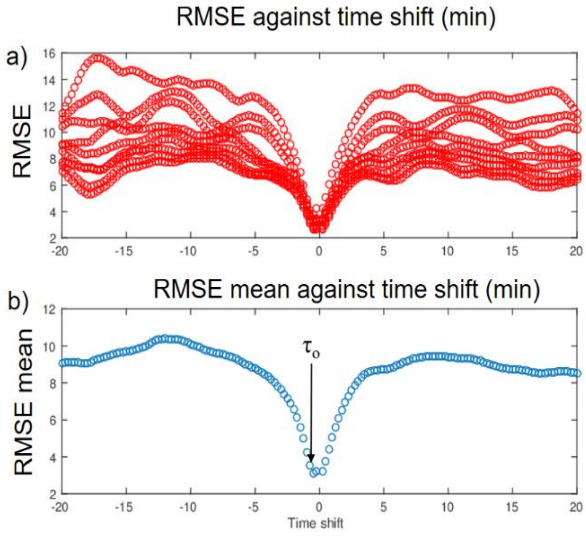

Figure 11. Plot of RMSE against time shift for Case 1. (a) RMSE of the 9 VOPs. (b) Mean RMSE of the 9 VOPs. Time shift with smallest RMSE was used as optimum time shift (τo=-0.5 min).

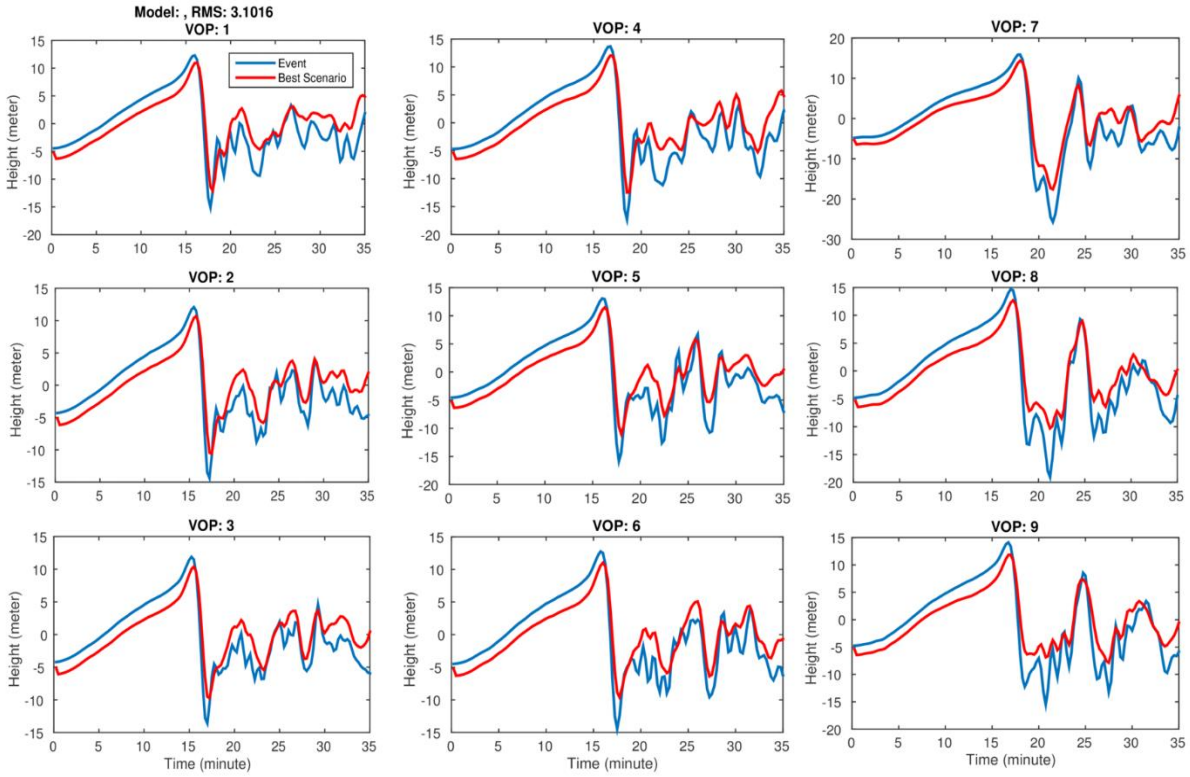

Figure 12. Comparison of tsunami waveforms at nine VOPs from the hypothetical megathrust earthquake Mw 9.0 (blue line) and fault model scenario No. 77 (red line) from the NearTIF database.

The optimum time shift (τ_o) approach enables us to find similar tsunami waveforms even if the fault models that produced these waveforms are different from scenarios. In this case, the optimum time shift to minimize the RMSE is -0.5 min. The pre-computed tsunami inundation from the best site-specific scenario (FMS No. 77) has the maximum tsunami height of 24.5 m and the maximum inundation distance inland in northern, central and southern Chimbote are approximately 3.6 km, 3.0 km and 3.8 km, respectively. The results of tsunami inundation obtained by the best fault model scenario are similar (in comparison) to the hypothetical fault model scenario (Mw 9.0) simulated by direct NFM which produces the maximum tsunami height of 34.3 m and inundation distances are 3.6 km, 3.2 km and 4.0 km, at the north, central and south of Chimbote, respectively (Figure 13a and 13b).

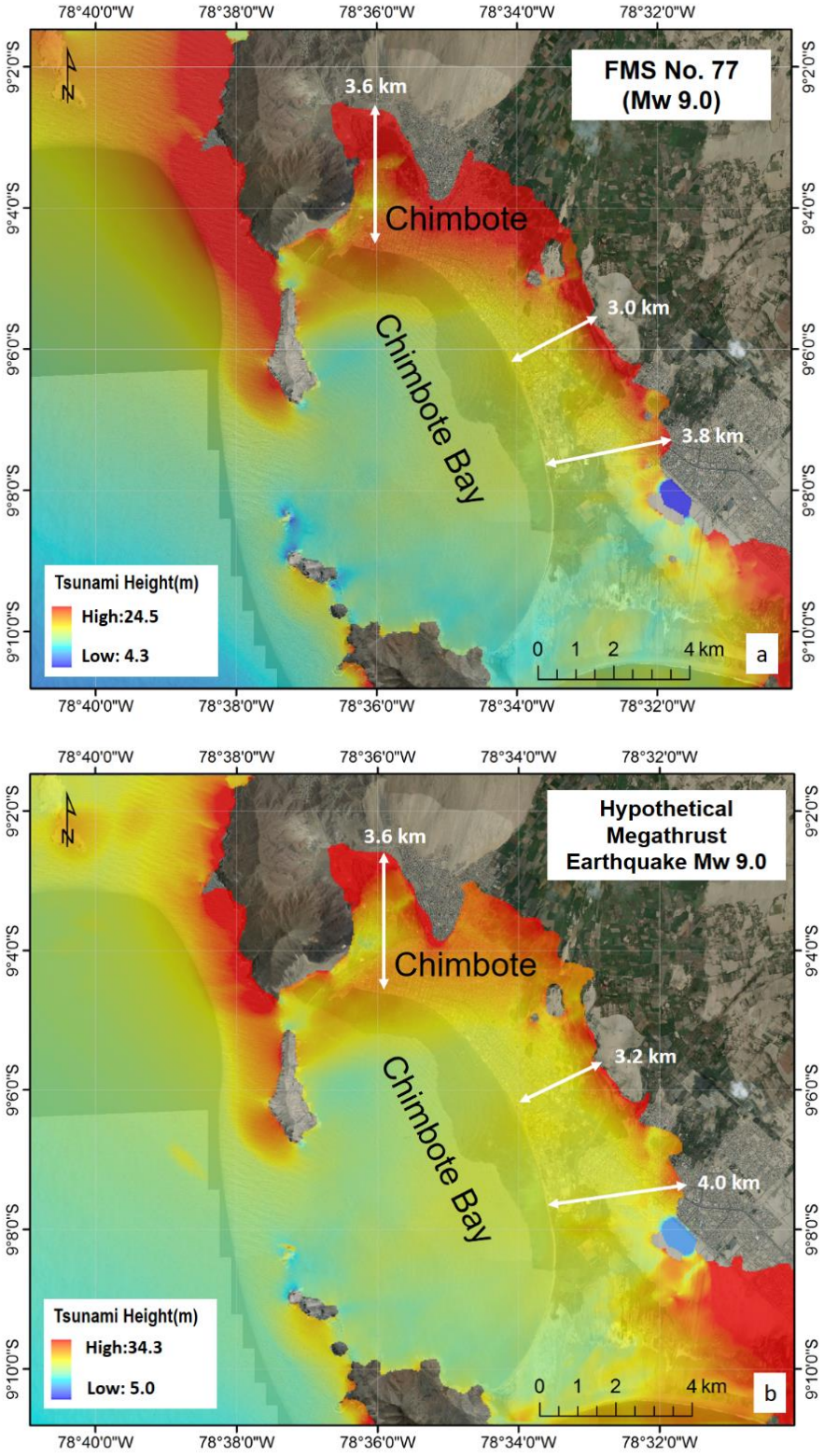

Figure 13. (a) Tsunami inundation forecasting of the best FMS No. 77 (Mw 9.0) in the NearTIF database. (b) Tsunami inundation forecasting from direct numerical forward modeling using the hypothetical scenario Mw 9.0.

The computational time for the inundation map by direct Numerical Forward Modeling (NFM) of 6 hours using JAGURS code takes approximately 45 min. The tsunami travel time (TTT) of the positive wave in each VOP located closer to the hypothetical earthquake (Mw 9.0) is between 20 min (VOP No. 2; 20 km off the coast of Chimbote) and 23 min (VOP No. 7; 11 km off coast Chimbote) after the earthquake occurred. The maximum amplitude is approximately 18 m after 2 hours of tsunami propagation, recorded at VOP No. 7 and VOP No. 8 (Figure C-1 in Appendix-C). At the virtual tide gauge of DHN "VTgDHN" (100 m off the coast of Chimbote) tsunamis will arrive with positive wave in 30 min and the maximum tsunami height of 19 m in 1 hour (Figure 14). If we compute tsunami inundation for Chimbote by numerical forward modeling even in the EIC high-performance computer (which takes 45 min) we would not have time to issue tsunami warning bulletins. By comparison, if we compute tsunami simulation using the NearTIF algorithm, it will take only 19 seconds, and less than 1 second to search the best site-specific fault model scenario (for this case the FMS No. 77). Also we would update the information about the seismic source delivered from national or international seismological institutes (for the case of Peru) which usually update the information within minutes or hours when an earthquake occurs, in order to be more reliable than the previous estimation. The CNAT in Peru, according to PO-SNAT thresholds established in 2012, do not have more than 10 minutes to issue the tsunami bulletins after receiving the information from the Geophysical Institute of Peru (IGP). In this sense, the NearTIF algorithm will be a good tool for implementation in CNAT for tsunami early warning.

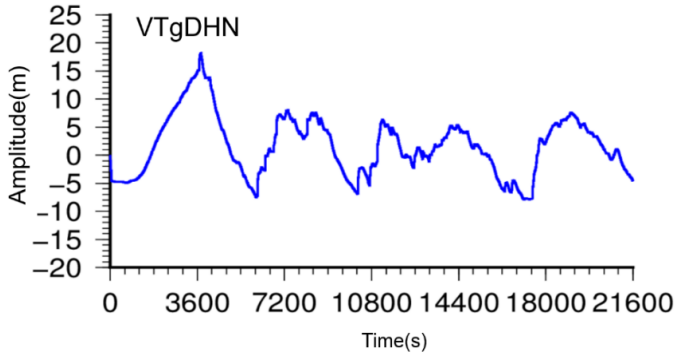

Figure 14. Computed nonlinear tsunami waveform for Mw 9.0 at virtual tide gauge of DHN "VTgDHN" offshore Chimbote. The maximum tsunami height was 19 m recorded at 1 hour.

4.3. Case 2: The Offshore Chimbote Hypothetical Thrust Earthquake (Mw 8.5)

A hypothetical megathrust earthquake (Mw 8.5) was used as a simple fault model scenario for offshore Chimbote (53 km off coast Chimbote) as a near-field tsunami case (Figure 15). The best site-specific

scenario calculated with the NearTIF algorithm is FMS No. 73 (Mw 8.6). The RMSE is 1.07 m and the optimum time shift (τ_o) is 1.25 min (Figure 16a and 16b). In spite that the magnitude obtained from the best scenario is slightly greater than the hypothetical scenario (Mw 8.5), the important point is that the tsunami waveform from the best scenario matches very well with the tsunami waveform from the hypothetical earthquake (Figure 17). The maximum tsunami inundation height of the best site-specific scenario is 14.5 m and the maximum inundation distances inland for northern, central and southern Chimbote are approximately 2.1 km, 0.8 km and 2.4 km, respectively.

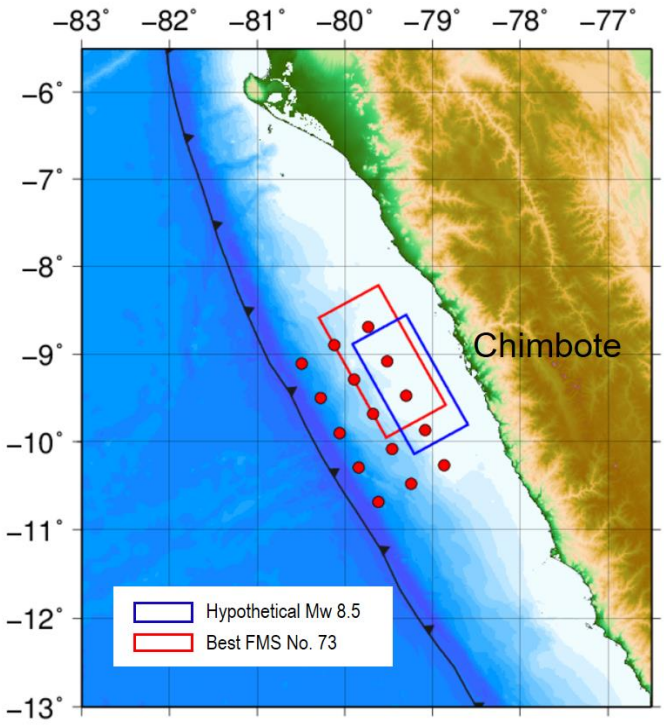

Figure 15. Location of hypothetical megathrust earthquake Mw 8.5 (blue rectangle) and the best FMS No. 73 (red rectangle).

The results of tsunami inundation obtained by the best-site specific fault model scenario are similar to that from the hypothetical fault model (Mw 8.5) simulated by direct NFM which produces the maximum tsunami height of 13.2 m and inundation distances of 2.2 km, 0.8 km and 2.6 km at the north, central and south of Chimbote (Figure 18a and 18b). It took approximately 40 min to compute the six hours (6h) tsunami propagation for the hypothetical scenario (Mw 8.5) using the JAGURS code. The TTT of the positive wave at the VOP closer to this event is 24 min (VOP No. 2; 20 km off coast Chimbote) and 30 min (VOP No. 7; 11 km off coast Chimbote) after the earthquake occurred. In Appendix-B, Table B-2 and Figure B-2 show the fault model parameters and vertical displacement of FMS No. 73 and hypothetical thrust earthquake Mw 8.5. The first tsunami amplitude of 5 m will reach

in 50 min at VOP No. 7 and the maximum amplitude registered at VOP No. 7 is 8 m after 2 hours of tsunami propagation (Figure C-2 in Appendix-C). At the "VTgDHN" tsunamis will arrive with positive wave in 40 min and the maximum tsunami height of 8.7 m at 1 hour, approximately (Figure 19). The computation time using the NearTIF took only 18 seconds and searching the best site-specific scenario took less than 2 seconds, which means only 20 seconds to obtain a tsunami inundation forecast map based on the best site-specific fault model scenario (FMS) No. 73.

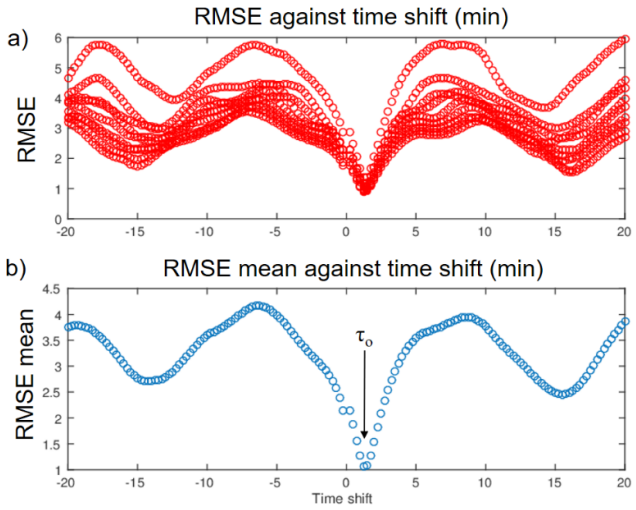

Figure 16. Plot of RMSE against time shift for Case 2. (a) RMSE for 9 VOPs. (b) Mean RMSE of the 9 VOP. Time shift with smallest RMSE (1.075 m) was used as optimum time shift (τo=1.25 min).

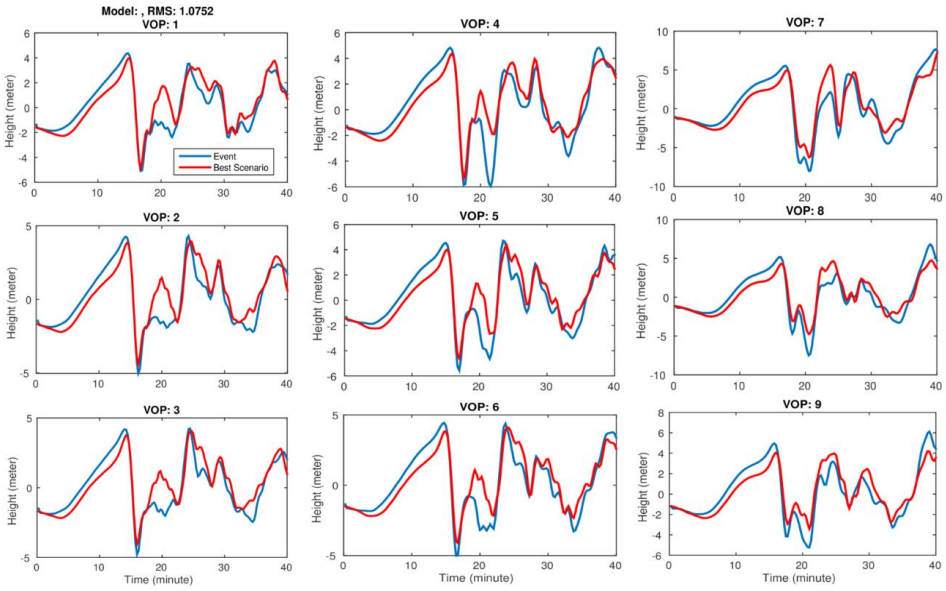

Figure 17. Comparison of tsunami waveforms of a hypothetical thrust earthquake Mw 8.5 (blue line) and fault model scenario No. 73 (red line) from the NearTIF database.

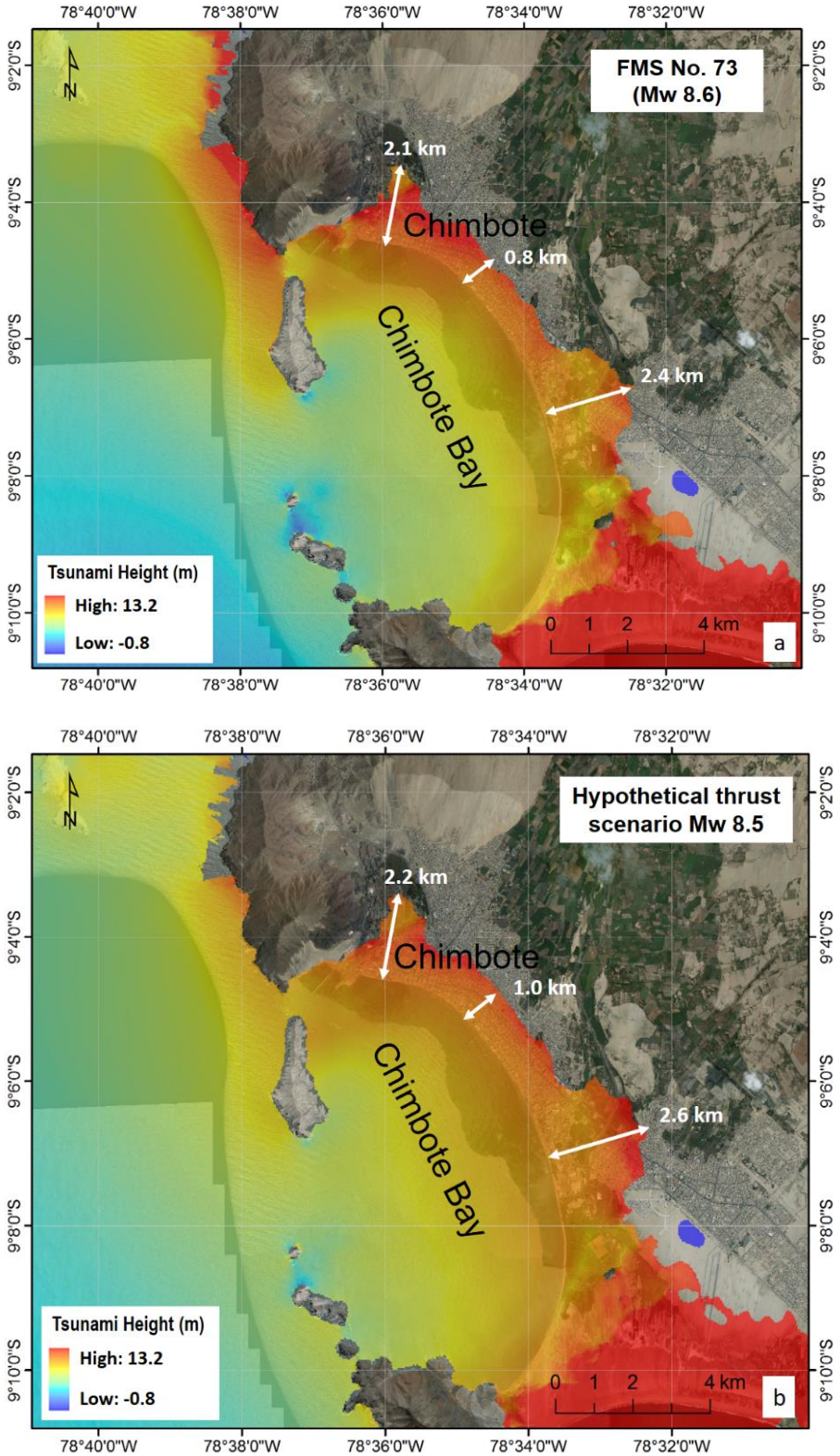

Figure 18. (a) Tsunami inundation forecasting of the best FMS No. 73 (Mw 8.6) in the NearTIF database. (b) Tsunami inundation forecasting from direct numerical forward modeling using a hypothetical scenario of Mw 8.5.

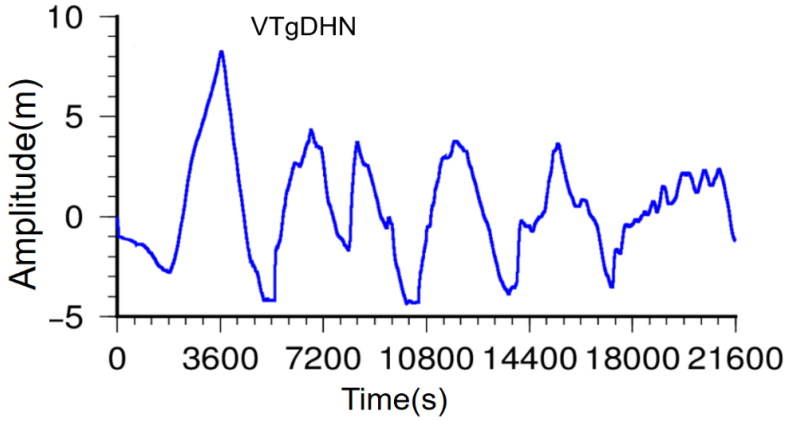

Figure 19. Computed nonlinear tsunami waveform for Mw 8.5 at virtual tide gauge of DHN "VTgDHN" offshore Chimbote. The maximum tsunami height of 8.7 m was recorded at approximately 1 hour.

4.4. Case 3: The 1996 Chimbote Tsunami Earthquake (Mw 7.6)

There is a finite fault model of tsunami earthquake (Mw 7.6) occurred in 1996 offshore Chimbote (rectangles in yellow color in Figure 9). This tsunami earthquake is characterized by "an earthquake that produces a large size tsunami relative to the value of its surface wave magnitude" (Kanamori, 1972; Jascha and Kanamori, 2009). In Appendix-B, Table B-3 and Figure B-3 show the heterogeneous models of 28 sub-faults by using teleseismic waveform inversion (Jimenez et al., 2015). Fault model scenario No. 122 (Mw 8.0) from the tsunami database is selected as the best site-specific scenario (Figure 20). The result by using the NearTIF method indicates the smallest RMSE value (0.123 m) and optimum time shift (τ_o=0.25 min) among tsunami waveforms at nine VOPs (Figure 21a and 21b). The selected fault model scenario No. 122 has different source parameters and a different magnitude in comparison with the 1996 tsunami earthquake (Table B-4 in Appendix-B).

Although the tsunami earthquake model has multiple sub-faults in comparison with the best fault model scenario, the difference is not important for the NearTIF algorithm because it searches and compares the tsunami waveforms to match very well after shifting the time. The similarity between the simulated tsunami waveforms from the tsunami earthquake and fault model scenario No. 122 is shown in Figure 22. The vertical displacement for the FMS No. 122 is shown in Appendix-B, Figure B-4.

The computational time for 6 hours of tsunami propagation was 27 min by numerical forward modeling (NFM). The maximum tsunami height is 5.4 m and its inundation distances are 0.2 km, 0.35 km and 0.21 km at the north, central and south of Chimbote, respectively (Figure 23). Satake and Tanioka (1999) indicated that measured tsunami height was 5 m above mean sea level from the

1996 Chimbote tsunami earthquake. The TTT is 1 hour at VOP No. 7 and the maximum tsunami amplitude is 2.5 m at 1 hour and 15 min (Figure C-3 in Appendix-C). The NearTIF method only took 14 seconds for linear long wave computation and searching the best scenario took less than 1 second. The best site-specific fault model scenario (FMS No. 122) has a tsunami height of 6.1 m and the similar values of inundation distance inland to the 1996 tsunami earthquake (Figure 23a and 23b). If we use the NearTIF method for this special event, we would have time to issue tsunami warning bulletins for evacuation and also to update tsunami inundation forecast maps.

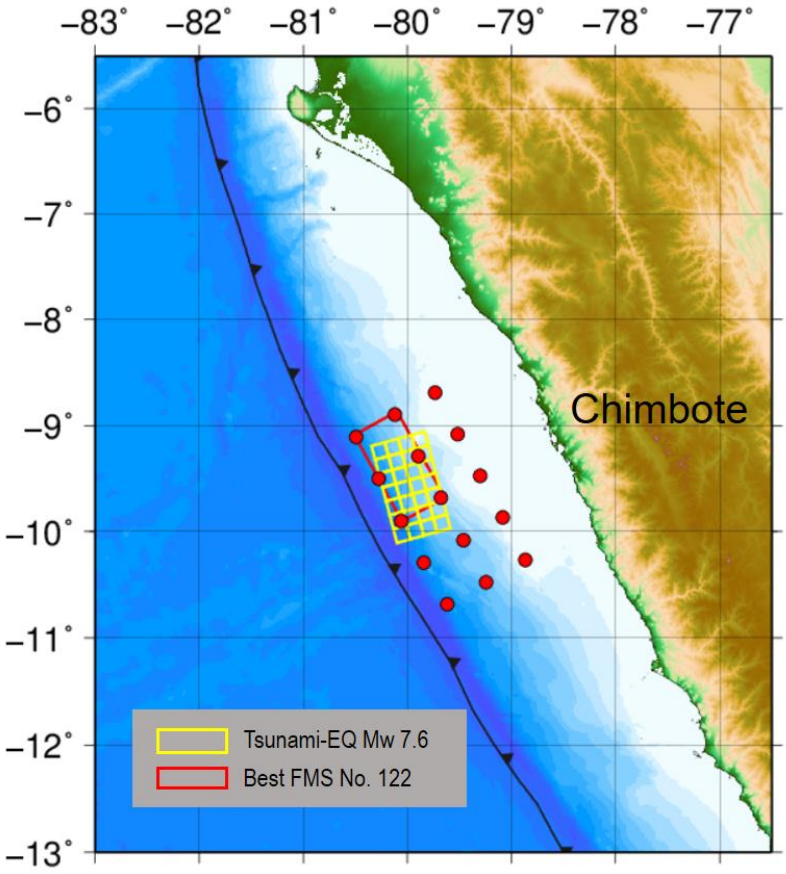

Figure 20. Location of tsunami earthquake scenario Mw 7.6 (yellow rectangle) and the best FMS No. 122 (red rectangle).

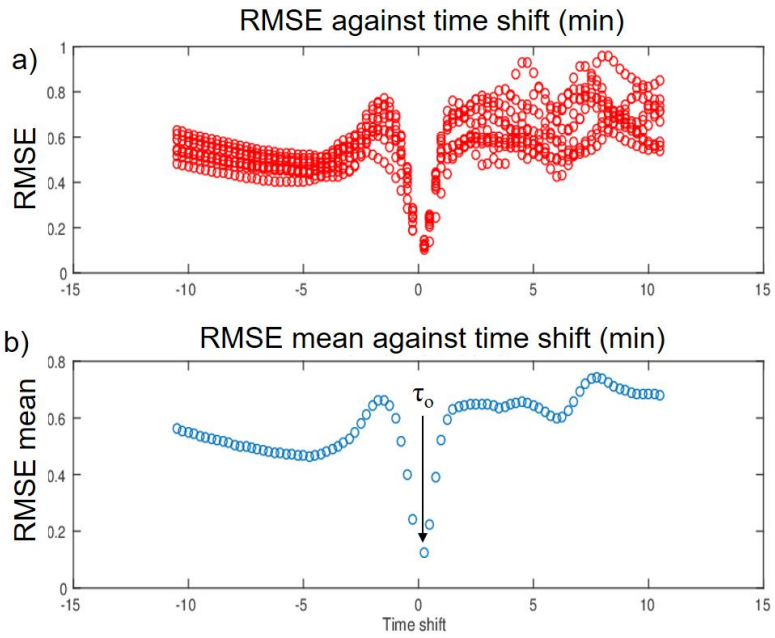

Figure 21. Plot of RMSE against time shift for Case 3. (a) RMSE for 9 VOPs. (b) Mean RMSE of the 9 VOPs. Time shift with smallest RMSE was used as optimum time shift (τo=0.25 min).

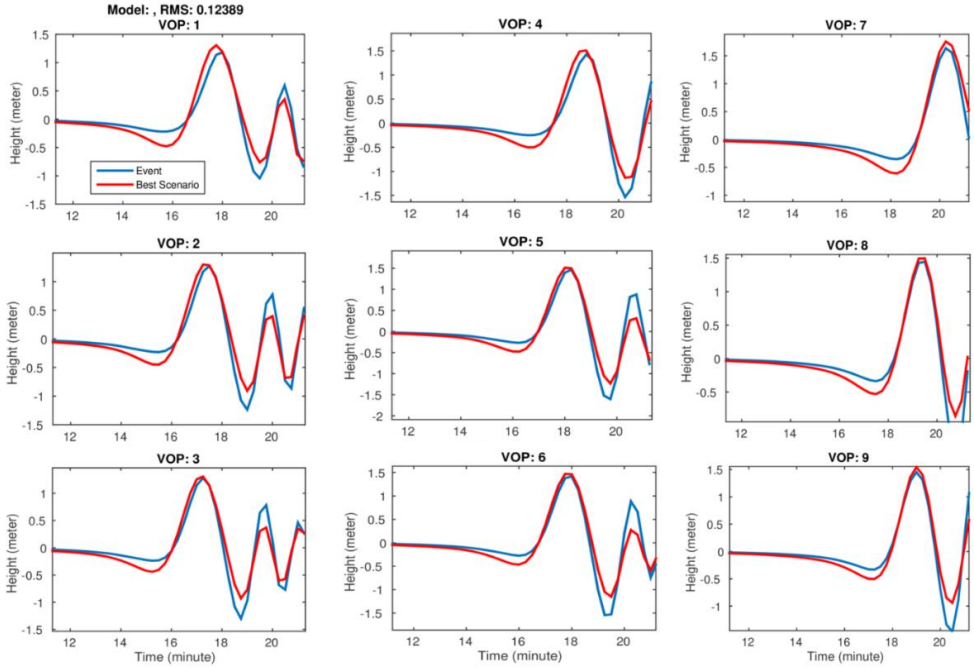

Figure 22. Comparison of tsunami waveforms at nine VOPs of the 1996 Chimbote tsunami earthquake Mw 7.6 in blue line and the best fault model scenario No. 122 in red line from the NearTIF database.

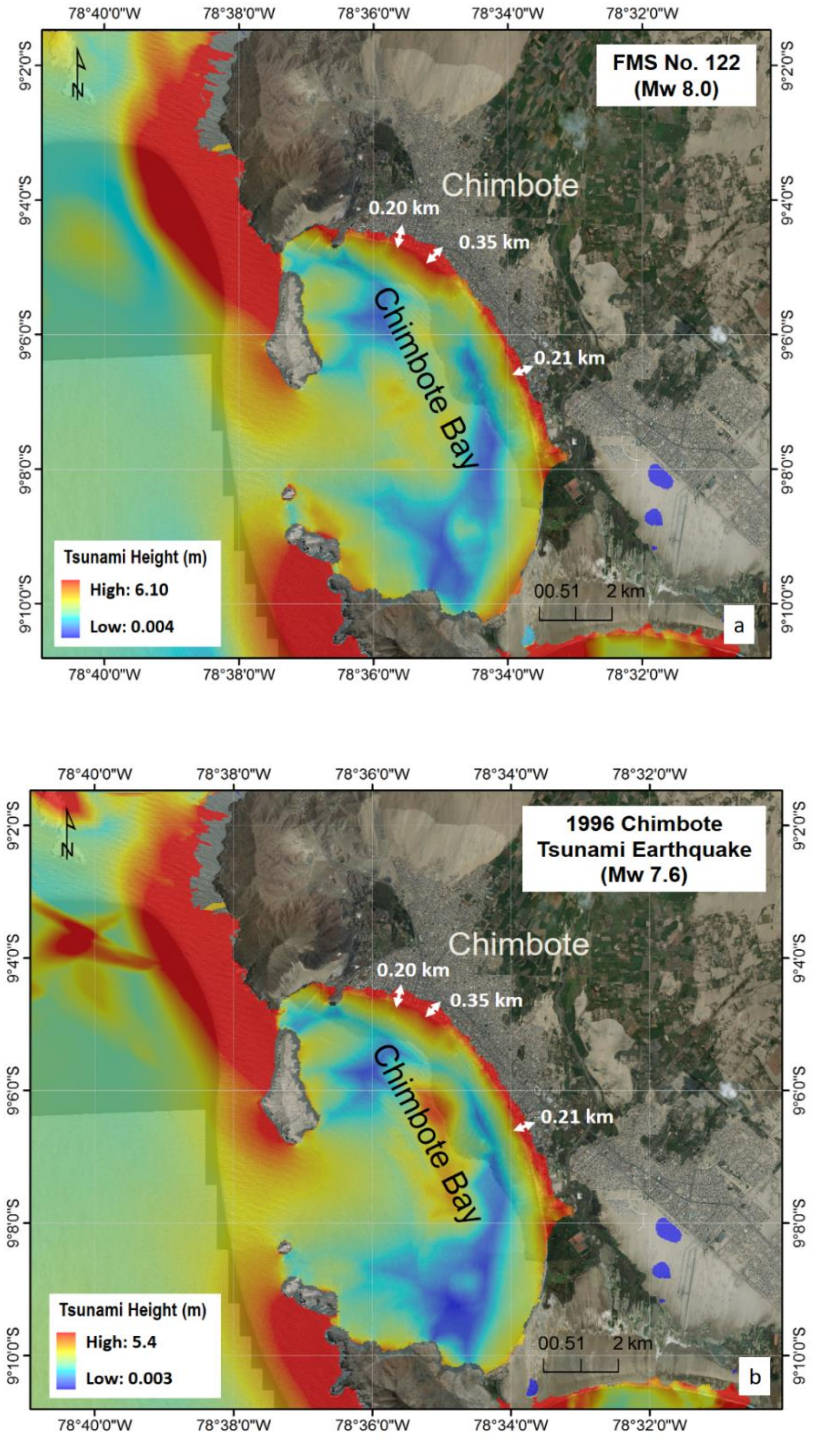

Figure 23. (a) Tsunami inundation forecasting of the best FMS No. 122 (Mw 8.0) in the NearTIF database. (b) Tsunami inundation forecasting from direct numerical forward modeling using the 1996 Chimbote tsunami earthquake scenario (Mw 7.6).

5. CONCLUSIONS

We performed the tsunami simulation using NearTIF algorithm for real-time tsunami inundation forecast with a focus on Chimbote city, Ancash Department, Peru. The pre-compute tsunami inundation database was built for 165 fault model scenarios from Mw 8.0 – 9.0 with an increment of 0.1 on the moment magnitude scale. We tested the effectiveness of NearTIF algorithm during 6 hours of tsunami propagation time using the JAGURS code with three types of earthquakes scenarios: two hypothetical megathrust earthquakes (Mw 9.0 and Mw 8.5) considered as near-field scenarios, and scenario for a tsunami earthquake which occurred in Chimbote in 1996 (Mw 7.6).

We compared the results of tsunami inundation for each hypothetical scenario with the obtained best-site specific fault model scenario. The comparison is done in terms of tsunami inundation distances for the north, central and southern Chimbote, respectively. For the hypothetical Mw 9.0 scenario, we obtained the maximum tsunami height of 34.3 m, the maximum inundation distances of 4.0 km in the southern part, and the tsunami travel time (TTT) of the positive wave is 20 min (VOP No. 2; 20 km off coast Chimbote) and 23 min (VOP No. 7; 11 km off coast Chimbote) after the earthquake occurrence. Nonlinear computation at virtual tide gauge of DHN "VTgDHN" offshore Chimbote recorded the maximum tsunami height of 19 m at 1 hour. For the hypothetical Mw 8.5 scenario, we obtained the maximum tsunami height of 13.2 m, the maximum inundation distances of 2.6 km in the southern part, and the TTT of the positive wave at 24 min (VOP No. 2) and 30 min (VOP No. 7) after the earthquake occurrence. Nonlinear computation at "VTgDHN" offshore Chimbote recorded the maximum tsunami height of 8.7 m at 1 hour. In both scenarios, the southern Chimbote is the most vulnerable area in terms of tsunami inundation and has very short time for tsunami evacuation. On the other hand, the results of the 1996 tsunami earthquake indicate a maximum tsunami height of 5.4 m and maximum inundation distance of 0.35 km in the central Chimbote, respectively. Satake and Tanioka (1999) indicated that a tsunami height was 5 m above the mean sea level in the 1996 Chimbote tsunami earthquake, which implies that the source model is a good approximation of the field survey in 1996 conducted by Bourgeois et al. (1999). The TTT of the positive wave is 1 hour at VOP No. 7 and the maximum tsunami amplitude is 2.5 m at 1 hour 15 min. Because a tsunami earthquake is relatively small in magnitude and rupture velocity, it can trigger a big impact along the coast. In this case, the people in Chimbote will have enough time for evacuation according to the obtained results.

Finally, we evaluated the lead time with NearTIF algorithm for the three earthquake scenarios. The computation time in the EIC high-performance computer indicated that we needed only less than 20 seconds to obtain a tsunami inundation forecast for Chimbote, in comparison with direct

numerical forward modeling (40-45 min) for the events Mw 8.5 and Mw 9.0. NearTIF method took only 14 seconds for linear shallow water wave computation and less than 1 second searching the best-fit fault model scenario for the 1996 tsunami earthquake event Mw 7.6 in comparison with 27 min by numerical forward modeling. The speed of the NearTIF algorithm to obtain the tsunami inundation forecast is remarkably (hundreds of times) faster than that by numerical forward modeling (NFM) computed in a EIC high-performance computer, Earthquake Research Institute, The University of Tokyo.

We conclude that we can apply NearTIF algorithm for the Peruvian Tsunami Warning Center and/or National Civil Defense (INDECI), because one advantage is to give enough time to issue tsunami warning bulletin to evacuate people and also to update the tsunami inundation forecast map due to a rapid estimation of tsunami inundation during a tsunamigenic event. We demonstrate that this methodology is reliable and useful for purpose of tsunami warning forecasting in Chimbote (as well as Tsunami Warning Center in Indonesia).

6. ACTION PLAN

We intend to increase the reliability and performance of the NearTIF algorithm for Chimbote city and notice the importance to carry out more tests with historical earthquakes scenarios. It implies the extension of the NearTIF coverage (such as to extend virtual observations points) in the southern Chimbote.

The tsunami inundation and tsunami waveform database produced by the NearTIF algorithm for Chimbote city can be improved by increasing the number of scenarios in the database through adding another fault mechanism such as tsunami earthquakes, normal fault, reverse fault and so on.

After finalizing this study, we will take into consideration the expansion of NearTIF for the central (e.g. Lima) and southern Peru (e.g. Tacna) in order to compute tsunami simulation for these areas, which are also tsunami-prone cities in the coast of Peru. The implementation of JAGURS tsunami code (Baba et al., 2014) and the NearTIF algorithm (Gusman et al., 2014) in the Peruvian Tsunami Warning Center (CNAT) is an important task.

APPENDICES

Appendix-A

Table A-1. Parameters of fault model scenario for thrust earthquakes event (No. 1 – 165).

No. FMS	Mw	Length (km)	Width (km)	Depth (km)	Strike (°)	Dip (°)	Rake (°)	Slip (m)	Latitude (°)	Longitude (°)
1	8.0	103.3	51.7	26.5	331.0	14.0	90.0	5.9	-9.100238	-79.505585
2	8.1	112.7	56.3	26.5	331.0	14.0	90.0	7.0	-9.134932	-79.486049
3	8.2	122.8	61.4	26.5	331.0	14.0	90.0	8.3	-9.167464	-79.465651
4	8.3	133.9	66.9	26.5	331.0	14.0	90.0	9.9	-9.205236	-79.444460
5	8.4	146.0	73.0	26.5	331.0	14.0	90.0	11.8	-9.250611	-79.417448
6	8.5	159.1	79.6	26.5	331.0	14.0	90.0	14.0	-9.307322	-79.383360
7	8.6	173.5	86.7	26.5	331.0	14.0	90.0	16.6	-9.355753	-79.361913
8	8.7	189.1	94.6	26.5	331.0	14.0	90.0	19.7	-9.414730	-79.326692
9	8.8	206.2	103.1	26.5	331.0	14.0	90.0	23.5	-9.472011	-79.294022
10	8.9	224.8	112.4	26.5	331.0	14.0	90.0	27.9	-9.540161	-79.259396
11	9.0	245.1	122.5	26.5	331.0	14.0	90.0	33.1	-9.620475	-79.219170
12	8.0	103.3	51.7	27.8	331.0	14.0	90.0	5.9	-9.489256	-79.290726
13	8.1	112.7	56.3	27.8	331.0	14.0	90.0	7.0	-9.523950	-79.271190
14	8.2	122.8	61.4	27.8	331.0	14.0	90.0	8.3	-9.556482	-79.250792
15	8.3	133.9	66.9	27.8	331.0	14.0	90.0	9.9	-9.594254	-79.229601
16	8.4	146.0	73.0	27.8	331.0	14.0	90.0	11.8	-9.639628	-79.202589
17	8.5	159.1	79.6	27.8	331.0	14.0	90.0	14.0	-9.696340	-79.168501
18	8.6	173.5	86.7	27.8	331.0	14.0	90.0	16.6	-9.744771	-79.147054
19	8.7	189.1	94.6	27.8	331.0	14.0	90.0	19.7	-9.803748	-79.111833
20	8.8	206.2	103.1	27.8	331.0	14.0	90.0	23.5	-9.861029	-79.079163
21	8.9	224.8	112.4	27.8	331.0	14.0	90.0	27.9	-9.929179	-79.044537
22	9.0	245.1	122.5	27.8	331.0	14.0	90.0	33.1	-10.00943	-79.004311
23	8.0	103.3	51.7	27.5	331.0	14.0	90.0	5.9	-9.877958	-79.073658
24	8.1	112.7	56.3	27.5	331.0	14.0	90.0	7.0	-9.912652	-79.054123

Table A-1. Continued.

25	8.2	122.8	61.4	27.5	331.0	14.0	90.0	8.3	-9.945184	-79.033725
26	8.3	133.9	66.9	27.5	331.0	14.0	90.0	9.9	-9.982956	-79.012534
27	8.4	146.0	73.0	27.5	331.0	14.0	90.0	11.8	-10.02831	-78.985522
28	8.5	159.1	79.6	27.5	331.0	14.0	90.0	14.0	-10.08504	-78.951433
29	8.6	173.5	86.7	27.5	331.0	14.0	90.0	16.6	-10.13347	-78.929986
30	8.7	189.1	94.6	27.5	331.0	14.0	90.0	19.7	-10.19245	-78.894765
31	8.8	206.2	103.1	27.5	331.0	14.0	90.0	23.5	-10.24973	-78.862096
32	8.9	224.8	112.4	27.5	331.0	14.0	90.0	27.9	-10.31788	-78.827469
33	9.0	245.1	122.5	27.5	331.0	14.0	90.0	33.1	-10.39819	-78.787244
34	8.0	103.3	51.7	27.0	331.0	15.0	90.0	5.9	-10.27169	-78.855847
35	8.1	112.7	56.3	27.0	331.0	15.0	90.0	7.0	-10.30638	-78.836311
36	8.2	122.8	61.4	27.0	331.0	15.0	90.0	8.3	-10.33892	-78.815913
37	8.3	133.9	66.9	27.0	331.0	15.0	90.0	9.9	-10.37669	-78.794722
38	8.4	146.0	73.0	27.0	331.0	15.0	90.0	11.8	-10.42206	-78.767710
39	8.5	159.1	79.6	27.0	331.0	15.0	90.0	14.0	-10.47877	-78.733622
40	8.6	173.5	86.7	27.0	331.0	15.0	90.0	16.6	-10.52721	-78.712174
41	8.7	189.1	94.6	27.0	331.0	15.0	90.0	19.7	-10.58618	-78.676954
42	8.8	206.2	103.1	27.0	331.0	15.0	90.0	23.5	-10.64346	-78.644284
43	8.9	224.8	112.4	27.0	331.0	15.0	90.0	27.9	-10.71161	-78.609658
44	9.0	230.9	115.4	27.0	331.0	15.0	90.0	27.6	-10.73508	-78.593506
45	8.0	103.3	51.7	29.0	331.0	17.0	90.0	5.9	-10.66543	-78.633846
46	8.1	112.7	56.3	29.0	331.0	17.0	90.0	7.0	-10.70012	-78.614311
47	8.2	122.8	61.4	29.0	331.0	17.0	90.0	8.3	-10.73265	-78.593913
48	8.3	133.9	66.9	29.0	331.0	17.0	90.0	9.9	-10.77042	-78.572722
49	8.4	146.0	73.0	29.0	331.0	17.0	90.0	11.8	-10.81580	-78.545709
50	8.5	159.1	79.6	29.0	331.0	17.0	90.0	14.0	-10.87251	-78.511621
51	8.6	173.5	86.7	29.0	331.0	17.0	90.0	16.6	-10.92094	-78.490174
52	8.7	189.1	94.6	29.0	331.0	17.0	90.0	19.7	-10.97992	-78.454953
53	8.8	206.2	103.1	29.0	331.0	17.0	90.0	23.5	-11.03720	-78.422283
54	8.9	224.8	112.4	29.0	331.0	17.0	90.0	27.9	-11.10535	-78.387657
55	9.0	245.1	122.5	29.0	331.0	17.0	90.0	33.1	-11.18566	-78.347431
56	8.0	103.3	51.7	17.0	331.0	11.0	90.0	5.9	-9.302934	-79.882472

Table A-1. Continued.

57	8.1	112.7	56.3	17.0	331.0	11.0	90.0	7.0	-9.337628	-79.862936
58	8.2	122.8	61.4	17.0	331.0	11.0	90.0	8.3	-9.370160	-79.842538
59	8.3	133.9	66.9	17.0	331.0	11.0	90.0	9.9	-9.407932	-79.821347
60	8.4	146.0	73.0	17.0	331.0	11.0	90.0	11.8	-9.453306	-79.794335
61	8.5	159.1	79.6	17.0	331.0	11.0	90.0	14.0	-9.510017	-79.760247
62	8.6	173.5	86.7	17.0	331.0	11.0	90.0	16.6	-9.558449	-79.738799
63	8.7	189.1	94.6	17.0	331.0	11.0	90.0	19.7	-9.617426	-79.703578
64	8.8	206.2	103.1	17.0	331.0	11.0	90.0	23.5	-9.674706	-79.670909
65	8.9	224.8	112.4	17.0	331.0	11.0	90.0	27.9	-9.742857	-79.636283
66	9.0	245.1	122.5	17.0	331.0	11.0	90.0	33.1	-9.823171	-79.596057
67	8.0	103.3	51.7	16.6	331.0	11.0	90.0	5.9	-9.696174	-79.670780
68	8.1	112.7	56.3	16.6	331.0	11.0	90.0	7.0	-9.730868	-79.651244
69	8.2	122.8	61.4	16.6	331.0	11.0	90.0	8.3	-9.763400	-79.630846
70	8.3	133.9	66.9	16.6	331.0	11.0	90.0	9.9	-9.801172	-79.609655
71	8.4	146.0	73.0	16.6	331.0	11.0	90.0	11.8	-9.846547	-79.582643
72	8.5	159.1	79.6	16.6	331.0	11.0	90.0	14.0	-9.903258	-79.548555
73	8.6	173.5	86.7	16.6	331.0	11.0	90.0	16.6	-9.951689	-79.527108
74	8.7	189.1	94.6	16.6	331.0	11.0	90.0	19.7	-10.01066	-79.491887
75	8.8	206.2	103.1	16.6	331.0	11.0	90.0	23.5	-10.06794	-79.459217
76	8.9	224.8	112.4	16.6	331.0	11.0	90.0	27.9	-10.13609	-79.424591
77	9.0	245.1	122.5	16.6	331.0	11.0	90.0	33.1	-10.21641	-79.384365
78	8.0	103.3	51.7	17.12	331.0	11.0	90.0	5.9	-10.09567	-79.446029
79	8.1	112.7	56.3	17.12	331.0	11.0	90.0	7.0	-10.13037	-79.426493
80	8.2	122.8	61.4	17.12	331.0	11.0	90.0	8.3	-10.16290	-79.406095
81	8.3	133.9	66.9	17.12	331.0	11.0	90.0	9.9	-10.20067	-79.384904
82	8.4	146.0	73.0	17.12	331.0	11.0	90.0	11.8	-10.24605	-79.357892
83	8.5	159.1	79.6	17.12	331.0	11.0	90.0	14.0	-10.30276	-79.323804
84	8.6	173.5	86.7	17.12	331.0	11.0	90.0	16.6	-10.35119	-79.302356
85	8.7	189.1	94.6	17.12	331.0	11.0	90.0	19.7	-10.41017	-79.267135
86	8.8	206.2	103.1	17.12	331.0	11.0	90.0	23.5	-10.46745	-79.234466
87	8.9	224.8	112.4	17.12	331.0	11.0	90.0	27.9	-10.53560	-79.199840
88	9.0	245.1	122.5	17.12	331.0	11.0	90.0	33.1	-10.61592	-79.159614

Table A-1. Continued.

89	8.0	103.3	51.7	16.6	331.0	11.0	90.0	5.9	-10.47227	-79.227826
90	8.1	112.7	56.3	16.6	331.0	11.0	90.0	7.0	-10.50696	-79.208290
91	8.2	122.8	61.4	16.6	331.0	11.0	90.0	8.3	-10.53949	-79.187892
92	8.3	133.9	66.9	16.6	331.0	11.0	90.0	9.9	-10.57726	-79.166701
93	8.4	146.0	73.0	16.6	331.0	11.0	90.0	11.8	-10.62264	-79.139689
94	8.5	159.1	79.6	16.6	331.0	11.0	90.0	14.0	-10.67935	-79.105601
95	8.6	173.5	86.7	16.6	331.0	11.0	90.0	16.6	-10.72778	-79.084153
96	8.7	189.1	94.6	16.6	331.0	11.0	90.0	19.7	-10.78676	-79.048933
97	8.8	206.2	103.1	16.6	331.0	11.0	90.0	23.5	-10.84404	-79.016263
98	8.9	224.8	112.4	16.6	331.0	11.0	90.0	27.9	-10.91219	-78.981637
99	9.0	245.1	122.5	16.6	331.0	11.0	90.0	33.1	-10.99250	-78.941411
100	8.0	103.3	51.7	17.2	331.0	14.0	90.0	5.9	-10.86965	-79.016766
101	8.1	112.7	56.3	17.2	331.0	14.0	90.0	7.0	-10.90434	-78.997230
102	8.2	122.8	61.4	17.2	331.0	14.0	90.0	8.3	-10.93688	-78.976832
103	8.3	133.9	66.9	17.2	331.0	14.0	90.0	9.9	-10.97465	-78.955641
104	8.4	146.0	73.0	17.2	331.0	14.0	90.0	11.8	-11.02002	-78.928629
105	8.5	159.1	79.6	17.2	331.0	14.0	90.0	14.0	-11.07673	-78.894541
106	8.6	173.5	86.7	17.2	331.0	14.0	90.0	16.6	-11.12517	-78.873094
107	8.7	189.1	94.6	17.2	331.0	14.0	90.0	19.7	-11.18414	-78.837873
108	8.8	206.2	103.1	17.2	331.0	14.0	90.0	23.5	-11.24142	-78.805203
109	8.9	224.8	112.4	17.2	331.0	14.0	90.0	27.9	-11.30957	-78.770577
110	9.0	245.1	122.5	17.2	331.0	14.0	90.0	33.1	-11.38989	-78.730351
111	8.0	103.3	51.7	11.0	331.0	6.0	90.0	5.9	-9.512743	-80.268710
112	8.1	112.7	56.3	11.0	331.0	6.0	90.0	7.0	-9.547436	-80.249175
113	8.2	122.8	61.4	11.0	331.0	6.0	90.0	8.3	-9.579968	-80.228777
114	8.3	133.9	66.9	11.0	331.0	6.0	90.0	9.9	-9.617740	-80.207586
115	8.4	146.0	73.0	11.0	331.0	6.0	90.0	11.8	-9.663115	-80.180573
116	8.5	159.1	79.6	11.0	331.0	6.0	90.0	14.0	-9.719826	-80.146485
117	8.6	173.5	86.7	11.0	331.0	6.0	90.0	16.6	-9.768257	-80.125038
118	8.7	189.1	94.6	11.0	331.0	6.0	90.0	19.7	-9.827234	-80.089817
119	8.8	206.2	103.1	11.0	331.0	6.0	90.0	23.5	-9.884515	-80.057147
120	8.9	224.8	112.4	11.0	331.0	6.0	90.0	27.9	-9.952665	-80.022521
121	9.0	245.1	122.5	11.0	331.0	6.0	90.0	33.1	-10.03298	-79.982295

Table A-1. Continued.

122	8.0	103.3	51.7	10.2	331.0	7.0	90.0	5.9	-9.903599	-80.049866
123	8.1	112.7	56.3	10.2	331.0	7.0	90.0	7.0	-9.938293	-80.030330
124	8.2	122.8	61.4	10.2	331.0	7.0	90.0	8.3	-9.970825	-80.009933
125	8.3	133.9	66.9	10.2	331.0	7.0	90.0	9.9	-10.00859	-79.988742
126	8.4	146.0	73.0	10.2	331.0	7.0	90.0	11.8	-10.05397	-79.961729
127	8.5	159.1	79.6	10.2	331.0	7.0	90.0	14.0	-10.11068	-79.927641
128	8.6	173.5	86.7	10.2	331.0	7.0	90.0	16.6	-10.15911	-79.906194
129	8.7	189.1	94.6	10.2	331.0	7.0	90.0	19.7	-10.21809	-79.870973
130	8.8	206.2	103.1	10.2	331.0	7.0	90.0	23.5	-10.27537	-79.838303
131	8.9	224.8	112.4	10.2	331.0	7.0	90.0	27.9	-10.34352	-79.803677
132	9.0	245.1	122.5	10.2	331.0	7.0	90.0	33.1	-10.42383	-79.763451
133	8.0	103.3	51.7	10.0	331.0	6.0	90.0	5.9	-10.29952	-79.832267
134	8.1	112.7	56.3	10.0	331.0	6.0	90.0	7.0	-10.33422	-79.812732
135	8.2	122.8	61.4	10.0	331.0	6.0	90.0	8.3	-10.36675	-79.792334
136	8.3	133.9	66.9	10.0	331.0	6.0	90.0	9.9	-10.40452	-79.771143
137	8.4	146.0	73.0	10.0	331.0	6.0	90.0	11.8	-10.44989	-79.744130
138	8.5	159.1	79.6	10.0	331.0	6.0	90.0	14.0	-10.50661	-79.710042
139	8.6	173.5	86.7	10.0	331.0	6.0	90.0	16.6	-10.55504	-79.688595
140	8.7	189.1	94.6	10.0	331.0	6.0	90.0	19.7	-10.61401	-79.653374
141	8.8	206.2	103.1	10.0	331.0	6.0	90.0	23.5	-10.67129	-79.620704
142	8.9	224.8	112.4	10.0	331.0	6.0	90.0	27.9	-10.73944	-79.586078
143	9.0	245.1	122.5	10.0	331.0	6.0	90.0	33.1	-10.81976	-79.545852
144	8.0	103.3	51.7	10.3	331.0	5.5	90.0	5.9	-10.69489	-79.608700
145	8.1	112.7	56.3	10.3	331.0	5.5	90.0	7.0	-10.72958	-79.589165
146	8.2	122.8	61.4	10.3	331.0	5.5	90.0	8.3	-10.76212	-79.568767
147	8.3	133.9	66.9	10.3	331.0	5.5	90.0	9.9	-10.79989	-79.547576
148	8.4	146.0	73.0	10.3	331.0	5.5	90.0	11.8	-10.84526	-79.520563
149	8.5	159.1	79.6	10.3	331.0	5.5	90.0	14.0	-10.90197	-79.486475
150	8.6	173.5	86.7	10.3	331.0	5.5	90.0	16.6	-10.95041	-79.465028
151	8.7	189.1	94.6	10.3	331.0	5.5	90.0	19.7	-11.00938	-79.429807
152	8.8	206.2	103.1	10.3	331.0	5.5	90.0	23.5	-11.06666	-79.397137
153	8.9	224.8	112.4	10.3	331.0	5.5	90.0	27.9	-11.13481	-79.362511

Table A-1. Continued.

154	9.0	245.1	122.5	10.3	331.0	5.5	90.0	33.1	-11.21513	-79.322285
155	8.0	103.3	51.7	10.9	331.0	7.0	90.0	5.9	-11.08423	-79.399428
156	8.1	112.7	56.3	10.9	331.0	7.0	90.0	7.0	-11.11892	-79.379893
157	8.2	122.8	61.4	10.9	331.0	7.0	90.0	8.3	-11.15145	-79.359495
158	8.3	133.9	66.9	10.9	331.0	7.0	90.0	9.9	-11.18923	-79.338304
159	8.4	146.0	73.0	10.9	331.0	7.0	90.0	11.8	-11.23460	-79.311291
160	8.5	159.1	79.6	10.9	331.0	7.0	90.0	14.0	-11.29131	-79.277203
161	8.6	173.5	86.7	10.9	331.0	7.0	90.0	16.6	-11.33974	-79.255756
162	8.7	189.1	94.6	10.9	331.0	7.0	90.0	19.7	-11.39872	-79.220535
163	8.8	206.2	103.1	10.9	331.0	7.0	90.0	23.5	-11.45600	-79.187865
164	8.9	224.8	112.4	10.9	331.0	7.0	90.0	27.9	-11.52415	-79.153239
165	9.0	245.1	122.5	10.9	331.0	7.0	90.0	33.1	-11.60446	-79.113013

Appendix-B

Table B-1. Parameters of the best fault model scenario No. 77 and hypothetical Chimbote earthquake Mw 9.0.

Parameter	Fault model scenario No. 77	Megathrust earthquake Mw 9.0
Magnitude	9.0	9.0
Strike angle	331	331
Dip angle	11	18
Rake angle	90	90
Rigidity (Nm^{-2})	4×10^{10}	4×10^{10}
Slip amount (m)	33.1	33.1
Length (km)	245.1	245.1
Width (km)	122.5	122.5
Top depth (km)	16.6	8.0

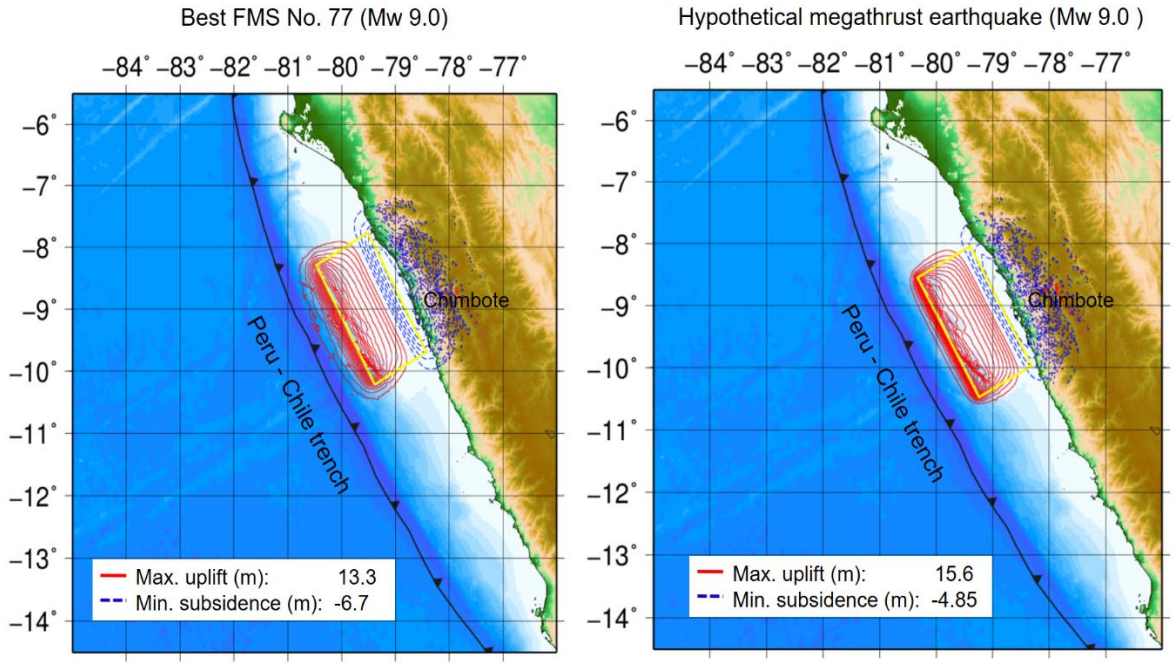

Figure B-1. Vertical displacement for the best FMS No. 77 (left) and hypothetical megathrust earthquake Mw 9.0 (right). Red contours show uplift with an interval of 1m. Blue dots contours show subsidence with an interval of 1m.

Table B-2. Parameters of the best fault model scenario No. 73 and hypothetical Chimbote earthquake Mw 8.5.

Parameter	Fault model scenario No. 73	Thrust earthquake Mw 8.5
Magnitude	8.6	8.5
Strike angle	331	331
Dip angle	11	16
Rake angle	90	90
Rigidity (Nm^{-2})	4×10^{10}	4×10^{10}
Slip amount (m)	14.0	16.0
Length (km)	159.1	173.5
Width (km)	79.6	86.7
Top depth (km)	10.0	16.6

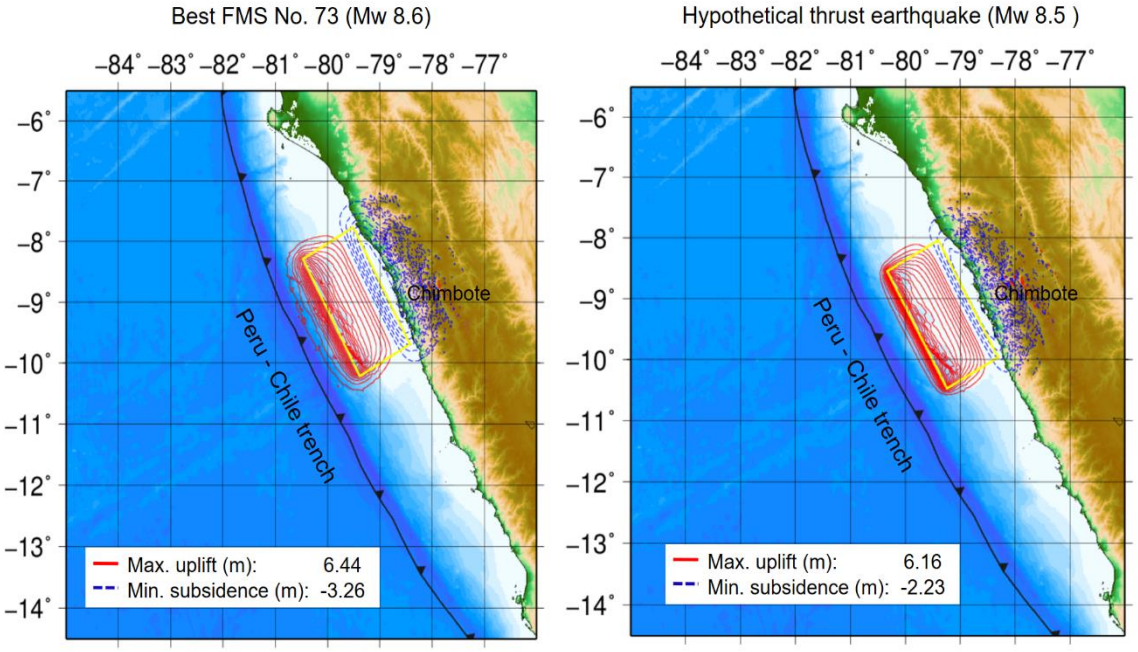

Figure B-2. Vertical displacement for the best FMS No. 73 (left) and hypothetical thrust earthquake Mw 8.5 (right). Red contours show uplift with an interval of 1m. Blue dots contours show subsidence with an interval of 1m.

Table B-3. Parameters of 1996 Chimbote tsunami earthquake Mw 7.6 (Jimenez et al., 2015).

No.	L (m)	W (m)	Top depth (m)	Strike (°)	Dip (°)	Rake (°)	Slip (m)	Lat (°)	Lon (°)
1	15000	15000	14240	345.0	12.0	59.98	2.09	-10.0035	-79.7156
2	15000	15000	11120	345.0	12.0	71.38	2.69	-10.0377	-79.8431
3	15000	15000	8000	345.0	12.0	73.76	2.08	-10.0718	-79.9706
4	15000	15000	4880	345.0	12.0	89.52	0.78	-10.1060	-80.0980
5	15000	15000	14240	345.0	12.0	70.28	1.77	-9.8732	-79.7506
6	15000	15000	11120	345.0	12.0	78.48	3.44	-9.9074	-79.8780
7	15000	15000	8000	345.0	12.0	76.99	4.23	-9.9415	-80.0055
8	15000	15000	4880	345.0	12.0	72.66	3.16	-9.9757	-80.1329
9	15000	15000	14240	345.0	12.0	109.18	2.25	-9.7429	-79.7855
10	15000	15000	11120	345.0	12.0	79.1	4.93	-9.7771	-79.9129
11	15000	15000	8000	345.0	12.0	76.19	6.62	-9.8112	-80.0404
12	15000	15000	4880	345.0	12.0	80.77	5.93	-9.8454	-80.1678
13	15000	15000	14240	345.0	12.0	96.05	2.86	-9.6126	-79.8204
14	15000	15000	11120	345.0	12.0	76.83	4.78	-9.6467	-79.9478
15	15000	15000	8000	345.0	12.0	72.7	6.52	-9.6809	-80.0753
16	15000	15000	4880	345.0	12.0	82.99	5.64	-9.7151	-80.2028
17	15000	15000	14240	345.0	12.0	87.17	2.00	-9.4823	-79.8553
18	15000	15000	11120	345.0	12.0	85.61	2.53	-9.5164	-79.9828
19	15000	15000	8000	345.0	12.0	69.92	3.61	-9.5506	-80.1102
20	15000	15000	4880	345.0	12.0	76.29	3.95	-9.5847	-80.2377
21	15000	15000	14240	345.0	12.0	97.37	1.59	-9.3520	-79.8902
22	15000	15000	11120	345.0	12.0	72.79	1.90	-9.3861	-80.0177
23	15000	15000	8000	345.0	12.0	50.35	2.50	-9.4203	-80.1451
24	15000	15000	4880	345.0	12.0	54.2	2.75	-9.4544	-80.2726
25	15000	15000	14240	345.0	12.0	64.57	1.48	-9.2217	-79.9251
26	15000	15000	11120	345.0	12.0	80.58	1.54	-9.2558	-80.0526
27	15000	15000	8000	345.0	12.0	62.28	1.51	-9.2900	-80.1800
28	15000	15000	4880	345.0	12.0	47.35	1.49	-9.3241	-80.3075

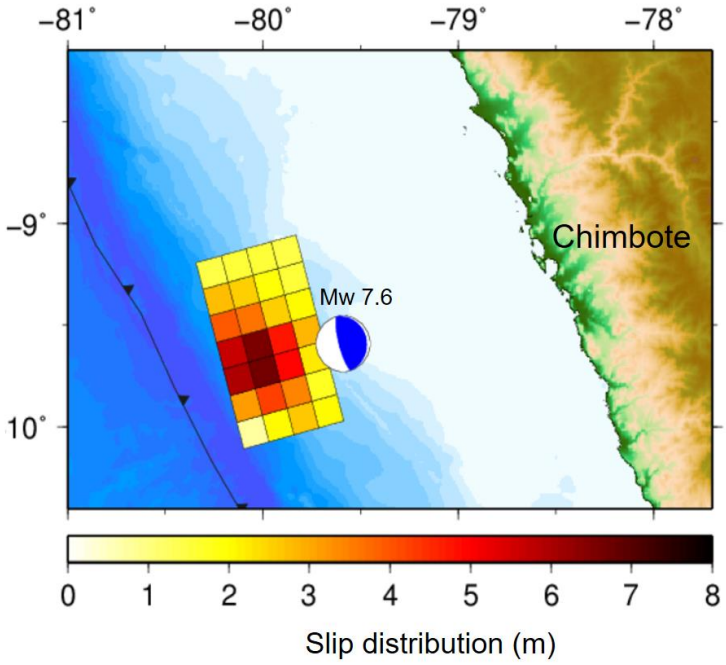

Figure B-3. Heterogeneous source model for 1996 Chimbote tsunami earthquake. Redrawn based on Jimenez et al. (2015).

Table B-4. Parameters of best fault model scenario No. 122.

Parameter	Fault model scenario No. 122
Magnitude	8.0
Strike angle	331
Dip angle	7.0
Rake angle	90
Rigidity (Nm^{-2})	4×10^{10}
Slip amount (m)	5.9
Length (km)	103.0
Width (km)	51.7
Top depth (km)	10.2

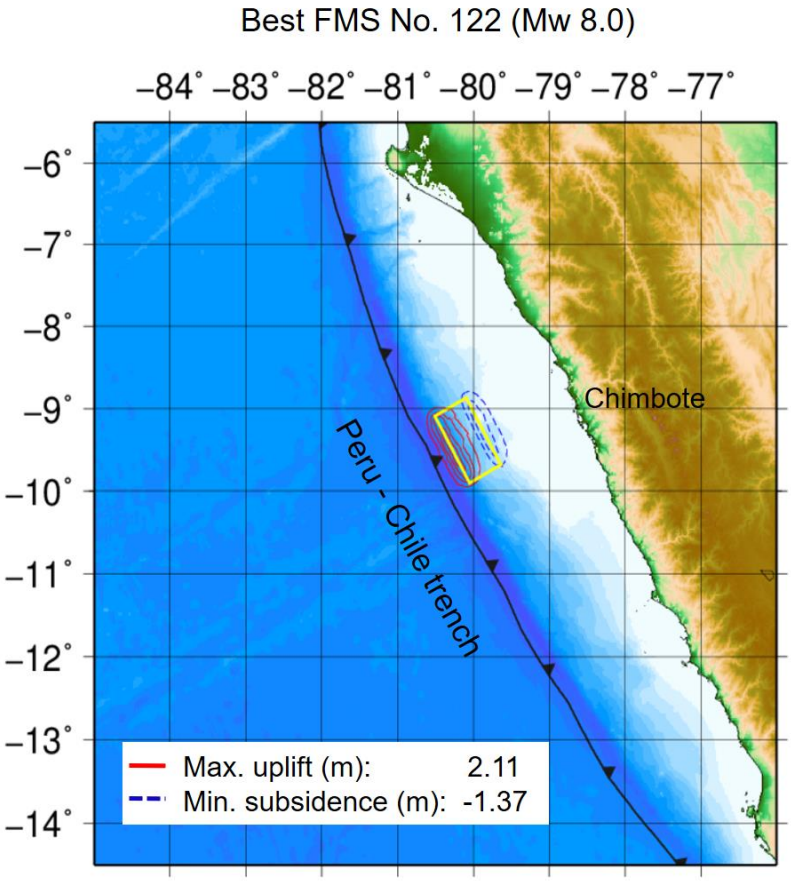

Figure B-4. Vertical displacement for the best FMS No. 122. Red contours show uplift with an interval of 0.5m. Blue dots contours show subsidence with an interval of 0.5 m.

Appendix-C

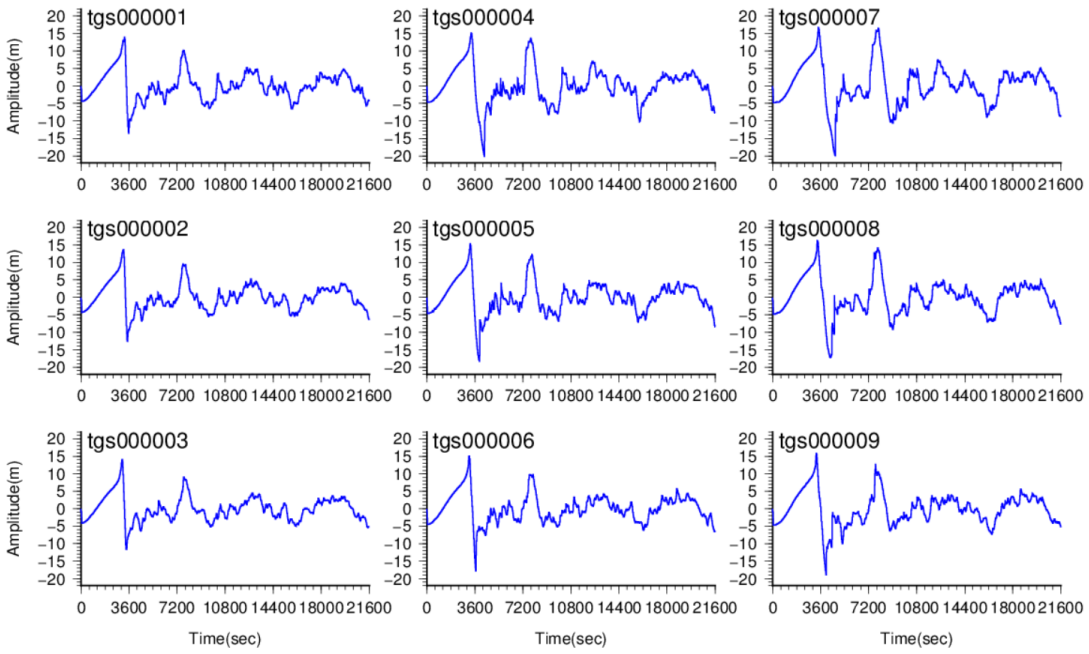

Figure C-1. Tsunami waveforms of hypothetical earthquake Mw 9.0.

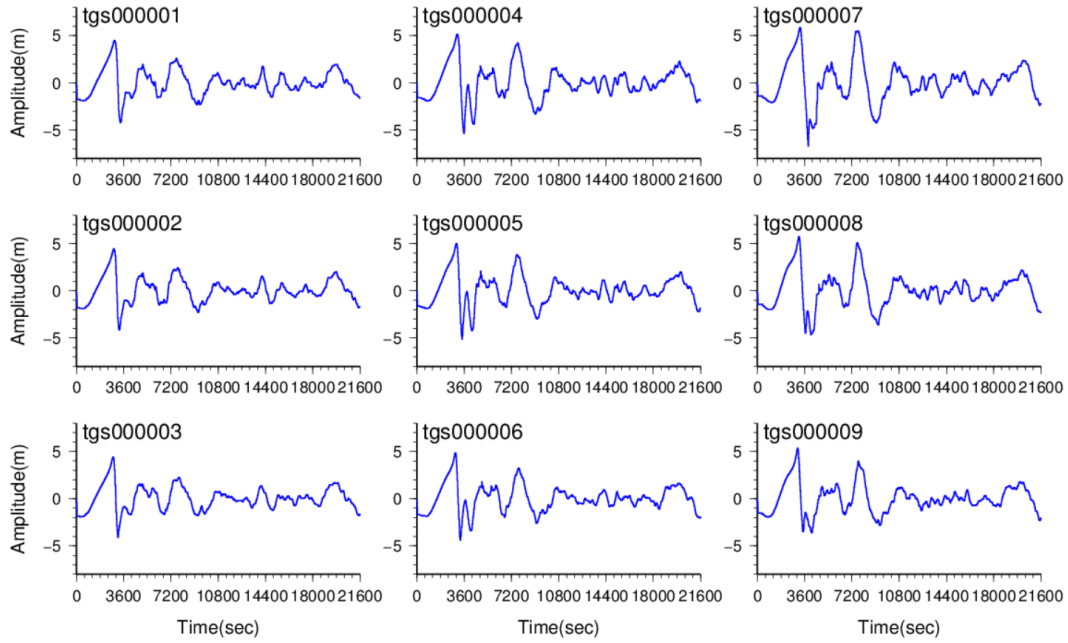

Figure C-2. Tsunami waveforms of hypothetical earthquake Mw 8.5.

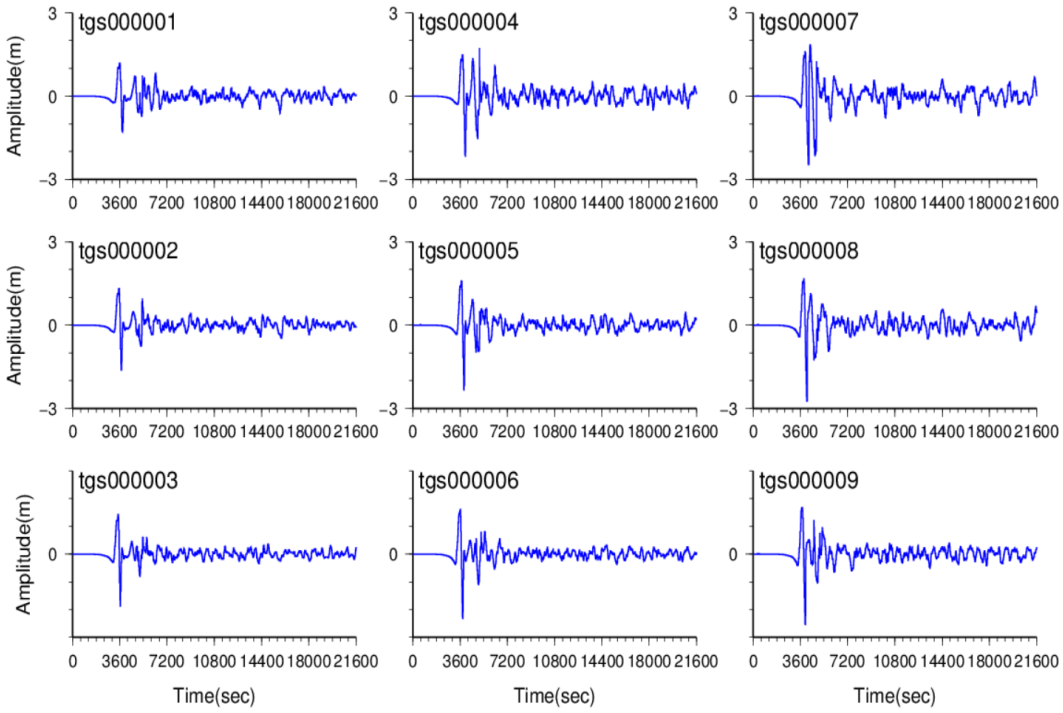

Figure C-3. Tsunami waveforms of the 1996 Chimbote tsunami earthquake Mw 7.6.

REFERENCES

Baba, T., N. Takahashi, Y. Kaneda, Y. Inazawa and M. Kikkojin., 2014, Tsunami inundation modeling of the 2011 Tohoku earthquake using three-dimensional building data for Sendai, Miyagi Prefecture, Japan, in V. S.-Fandiño et al. (ed.): Tsunami Events and Lessons Learned, Advances in Natural and Technological Hazards Research, Springer, 35, 89–98, doi: 10.1007/978 94-007-7269-4_3.

Baba, T., Cummins, P. R., 2016, JAGURS Users Guide, ver. 2016.10.24 Link: https://github.com/jagurs-admin/jagurs/blob/master/doc/JAGURS-User-Guide.En.pdf

Baba, T., Takahashi, N., Kaneda, Y., Ando, K., Matsuoka, D., Kato, T., 2015a, Parallel Implementation of Dispersive Tsunami Wave Modeling with a Nesting Algorithm for the 2011 Tohoku Tsunami. Pure Appl. Geophys. Doi 10.1007/s00024-015-1049-2.

Baba, T., Ando, K., Matsuoka, D., Hyodo, M., Hori, T., Takahashi, N., Obayashi, R., Imato, Y., Kitamura, D., Uehara, H., Kato, T., Saka, R., 2015b, Large-scale, high-speed tsunami prediction for Great Nankai Trough Earthquake on the K computer. The International Journal of High Performance Computing Applications 1-14 Doi: 10.1177/1094342015584090.

Bilek, S. L., 2010, Invited review paper: Seismicity along the South American subduction zone: Review of large earthquakes, tsunamis, and subduction zone complexity, Tectonophysics, 495(2), 2–14, doi:10.1016/j.tecto.2009.02.037.

Bourgeois, J., Petroff, C., Yeh, H., Titov, V., Synolakis, C., Benson, B., Kuroiwa, J., Lander, J., and Norabuena, E., 1999, Geologic setting, field survey and modeling of the Chimbote, northern Peru, tsunami of 21 February 1996, Pure Appl. Geophysics. 154(3/4), 513-540.

Dorbath, L., A. Cisternas, and C. Dorbath, 1990, Assessment of the size of large and great historical earthquakes in Peru, Bulletin of the Seismological Society of America, Vol. 80, No.3, pp. 551-576,1990.

Gusman, A. R., Y. Tanioka, B. T. MacInnes, and H. Tsushima, 2014, A methodology for near-field tsunami inundation forecasting: Application to the 2011 Tohoku tsunami, J. Geophys. Res. Solid Earth, 119, 8186–8206, doi:10.1002/2014JB010958.

Hanks, T. C., & Bakun, W. H., 2002, A bilinear source-scaling model for M-log A observations of continental earthquakes, Bulletin of the Seismological Society of America, 92(5), 1841–1846.

Hanks, T. C & Kanamori, H., 1979, A moment magnitude scale, Journal of Geophysical Research, Vol. 84, Issue B5, pp. 2348-2350. DOI: 10.1029/JB084iB05p02348.

Hayes, G. P., Wald, D. J., & Johnson, R. L., 2012, Slab1.0: A three-dimensional model of global subduction zone geometries. Journal of Geophysical Research, 117, B01302. doi:10.1029/ 2011JB008524.

Heinrich, P., Gomez, J.-M., Guibourg, S., and Ihmle, P. F., 1998, Modeling of the February 1996 Peruvian tsunami, Geophys. Res. Lett. 25(14), 2687-2690.

Ihmle, P. F., J.-M. Gomez, P. Heinrich, and S. Guibourg, 1998, The 1996 Peru tsunamigenic earthquake: Broadband source process, Geophys. Res. Lett., 25, 2691–2694, doi:10.1029/98GL01987.

Jarvis, A., H.I. Reuter, A. Nelson, E. Guevara, 2008, Hole-filled SRTM for the globe Version 4, available from the CGIAR-CSI SRTM 90m Database. Link (http://srtm.csi.cgiar.org/).

Jascha, P., H. Kanamori, 2009, Tsunami Earthquakes in Encyclopedia of Complexity and Systems Science, p. 967.

Jiménez, C., 2010, Software for determination of occurrence of tsunamis. Bol. Soc. Geol. Peru 104: 25-31. Sociedad Geologica del Perú SGP.

Jiménez, C., Calvo, M., & Tavera, H., 2015, Estudio numérico del sismo lento y maremoto de Chimbote 1996 (7.6 Mw). Revista de Investigación de Fisica, 18(1). Link: http://revistasinvestigacion.unmsm.edu.pe/index.php/fisica/article/view/11578/10384

Kanamori, H., 1972, Mechanism of tsunami earthquakes, Physics of the Earth and Planetary Interiors, 6: 346–359.

Kanamori, H., 1977, The energy release in great earthquakes, Journal of Geophysical Research, Vol. 82, issue 20, pp. 2981-2987. DOI: 10.1029/JB082i020p02981.

Kotani M, Imamura F. and Shuto N., 1998, Tsunami inundation calculation and damage estimation method using GIS. Proceedings of Coastal Engineering JSCE 45: 356–360.

Linsey, R. K. and J. B. Franzini, 1979, Eater–Resorurces Engineering, 3rd. Edition, MacGrawh–Hill Kogakusha Ltd., 716p.

Nishenko, S. P., 1991, Circum-Pacific seismic potential, U.S. Geological Survey, National Earthquake Information Center.

Okada, Y., 1985, Surface deformation due to shear and tensile faults in a half-space. Bulletin of the Seismological Society of America, 75(4), 1135–1154.

Pelayo, M. and Wiens, D., 1999, The November 20,1960 Peru Tsunami Earthquake: Source Mechanism of a slow event, Geophysical Research Letters, Vol 17 No. 6, 661-664.

Satake, K., Tanioka Y., 1999, Sources of Tsunami and Tsunamigenic Earthquakes in Subduction Zones, Volume 154, Issue 3–4, pp 467–483

Sawai, Y., Y. Namegaya, T. Tamura, R. Nakashima, and K. Tanigawa, 2015, Shorter intervals between great earthquakes near Sendai: Scour ponds and a sand layer attributable to A.D. 1454 overwash, Geophys. Res. Lett., 42, 4795–4800.

Secretaria de Gestion del Riesgo de Desastres, 2014, Plan Nacional de Gestion del Riesgo de Desastres Peru (PLANAGERD 2014- 2021).
Link http://www.preventionweb.net/files/37923_39462planagerd201420215b15d1.pdf

Setinoyo, U., Gusman, A., Satake, K., Fujii, Y., 2017, Pre-computed tsunami inundation database and forecast simulation in Pelabuhan Ratu, Indonesia, Pure and Applied Geophysics, Volume 174, Issue 8, pp 3219-3235.

Silgado, E., 1978, Historia de los sismos más notables ocurridos en el Perú (1513–1974), Geodinámica e Ingeniería Geológica, Serie C., vol. 3, edited by I. G. y Minería, Instituto de Geologia y Mineria, Perú, Lima.

Sistema Nacional de Alerta de Tsunamis, 2012, Protocolo Operativo de Sistema Nacional de Alerta de Tsunamis, First Edition.

Tanioka, Y., & Satake, K., 1996, Tsunami generation by horizontal displacement of ocean bottom. Geophysical Research Letters, 23, 861–864.

Tavera, H., and E. Buforn, 1998, Sismicidad y sismotectónica del Perú, Fis. la Tierra, 10, 187–219.

Villegas-Lanza, J. C., M. Chlieh, O. Cavalié, H. Tavera, P. Baby, J. Chire-Chira, and J.-M. Nocquet, 2016, Active tectonics of Peru: Heterogeneous interseismic coupling along the Nazca megathrust, rigid motion of the Peruvian Sliver, and Subandean shortening accommodation, J. Geophys. Res. Solid Earth, 121, doi:10.1002/2016JB013080.

Weatherall, P., Marks, K.M., Jakobsson, M., Schmitt, T., Tani, S., Arndt, J.E., Rovere, M., Chayes, D., Ferrini, V., & Wigley, R., 2015, A new digital bathymetric model of the world's oceans. *Earth and Space Science*, 2, 331–345, doi: 10.1002/ 2015EA000107.